The Application of Computational Fluid Dynamic Analysis to Jet Engine Inlet Flow Quality

Undergraduate Honors Thesis

Presented in Partial Fulfillment of the Requirements for

Graduation with Honors Research Distinction

in the Department of Mechanical and Aerospace Engineering at

The Ohio State University

By

Ryan W. Winfree

The Ohio State University

2013

Professor Richard J. Freuler, Advisor

Professor Clifford A. Whitfield, Advisor

Abstract

Damaging phenomena, such as the development of an inlet vortex, can occur on jet engines during various operational conditions on a taxiway. These vortices are anchored to the ground and extend into the inlet of the jet engine, and can have adverse effects on the engine by the lifting of debris into the engine and potentially damaging internal components. To analyze the flow effects caused by vortices, an engine simulator, a scale model of a jet engine, was operated at varying adverse operational conditions to understand which conditions will generate vortices. The engine simulator was run in a free field environment and at a height simulating the engine over a taxiway. The experimental mass flow results were compared to a computational model in Fluent, an existing computational fluid dynamic (CFD) program, which predicted the flow around the engine simulator. The preliminary results showed the correct flow structures for the free field environment. The free field CFD model was then adjusted to simulate the operating conditions of the engine over the taxiway. The CFD results produced a vortex forming from the ground to the engine. This information will provide a strong foundation and framework to build and expand the use of computational modeling in jet engine test simulations.

Dedication

Dedicated to Paige Reading, whose unwavering support allowed me to succeed

Acknowledgments

I would like to thank Dr. Freuler and Dr. Whitfield for being my advisors on this research project. The time and resources provided to me by them were invaluable and much appreciated. I have truly learned a lot through this research which was only possible due to the effort put in by my advisors.

To Jacob Allenstein, I would like to express my gratitude for all the help he gave in performing the experimental work at the Aeronautical and Astronautical Research Laboratories. I would also like to express gratitude to Greg Padgett and his advice in setting up my computational domain.

I appreciate all the support and encouragement from my family and friends along the way. A special thanks to Paige Reading and all the loving praise she provided throughout the entire research process. I am grateful for the funding provided to me by the college of engineering and the computing time allocated to me from the Ohio Supercomputer Center.

Table of Contents

List of Figures

List of Tables

Nomenclature

CFD	Computational Fluid Dynamics
CAD	Computer Aided Design
cf	Cubic feet
ANSA	Automatic Net-Generation for Structural Analysis
ANSYS	Analysis System
psi	Pounds per square inch
BM_{Dist}	Bellmouth distortion
BC	Boundary conditions
V_i	Engine velocity
V_o	Crosswind velocity
H	Engine centerline height
D	Engine inlet diameter
P_{max}	Max total pressure
P_{min}	Minimum total pressure
P_{avg}	Average total pressure
F.O.D.	Foreign Object Damage

Chapter 1: Introduction

1.1 Research Motivation

The formation of damaging vortices has been known to occur during the operation of a jet engine-powered aircraft on the taxiway. These standing vortices occur due to the short distance between the engine and the ground plane. The standing vortices are anchored to the ground and extend into the inlet of the jet engine as shown in Figure 1. As the vortex approaches the inlet, the vortex spirals with a decreasing radius of circular rotation with a lower pressure in the center of the vortex than the surrounding air [1, 2]. With the ingestion of this vortex, the engine's fan and compressor blades could be damaged. As the engine's vertical distance from the ground plane increases, the likelihood of vortex formation and its potential adverse effects start to diminish. Due to the fact that these standing vortices in the inlet of an engine can potentially cause severe damage to the jet engine, engine induced vortex formation has been an area of interest since the mid-1950s [3].

Figure 1: Vortex Visualized [4]

This chapter will briefly discuss how a vortex is formed and what damages may occur due to vortex formation. An overview of past investigations including what vortex formation prevention methods have been created will be provided, along with the goals of this research.

1.1.1 A General Review of Vortex Formation

A vortex is circular rotation about an axis. As shown in Figure 2, a vortex will have a higher fluid velocity in the center of the vortex with decreasing velocity moving radially outward. The longer vectors correspond to larger velocity magnitude in Figure 2 The characteristics of a vortex have been shown to be a function of engine centerline height (H), which is the distance between the center of the engine and the ground plane, engine thrust (V_i), wind velocity or ambient vorticity (V_o), and engine inlet diameter (D) [1-3]. These parameters are labeled on a general engine configuration in Figure 3.

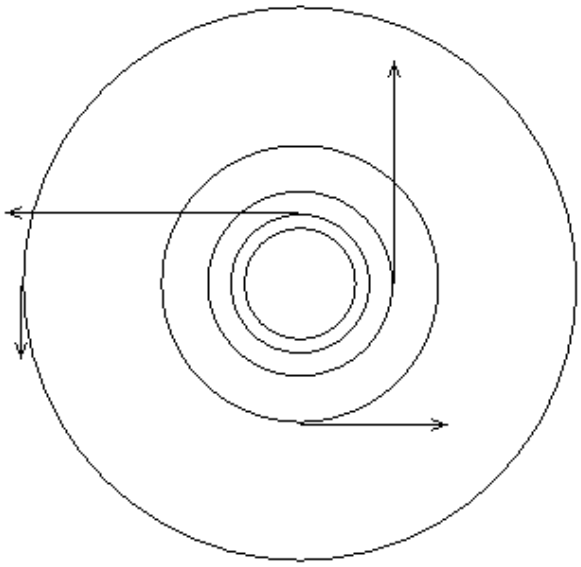

Figure 2: Vortex Top Down View [5]

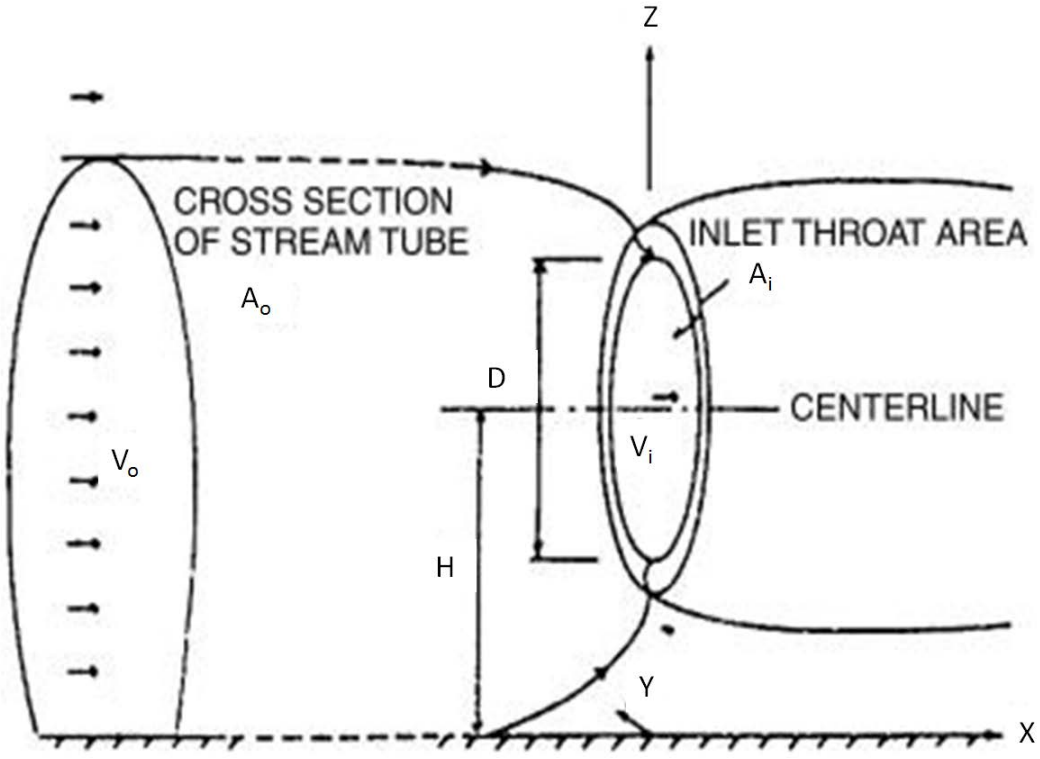

Figure 3: Vortex Formation Parameters [3]

When an engine is in operation, there is a volume of air in front of the engine that is affected by the engine flow. This volume of air is called a stream tube, which has a cross-sectional area A_o. When the engine centerline height is low enough to the ground, the stream tube will intersect with the ground plane as shown in Figure 3. Thus, the engine will induce a flow along the ground, and when combined with either ambient vorticity or a crosswind, creates the potential for a vortex to form [3].

Many investigators have quantified their results using two normalized parameters: $\frac{V_i}{V_o}$ and $\frac{H}{D_i}$, where the definition of each variable was given above [1-3]. The experimental results from previous research experiments have been graphed and are displayed in Figure 4. The solid line is an estimate of where vortex formation may occur. There have been variations in different studies on where this line should exactly be placed. W. H. Ho discusses why variations may have occurred among the studies [2]. However, the references this research is based on use the line in Figure 4, and thus this estimation will also be used here.

In order for a vortex to form, certain $\frac{V_i}{V_o}$ and $\frac{H}{D}$ conditions must be met. A vortex tends to form at high $\frac{V_i}{V_o}$ and low $\frac{H}{D}$ values. When $\frac{V_i}{V_o}$ is too low for a given $\frac{H}{D}$, no vortex will form, and the value for V_o is termed the "blow-away velocity". If a crosswind or headwind is too high the vortex will physically be blown away, and there will be no stagnation point at which the vortex would attach to the ground [1-3, 6].

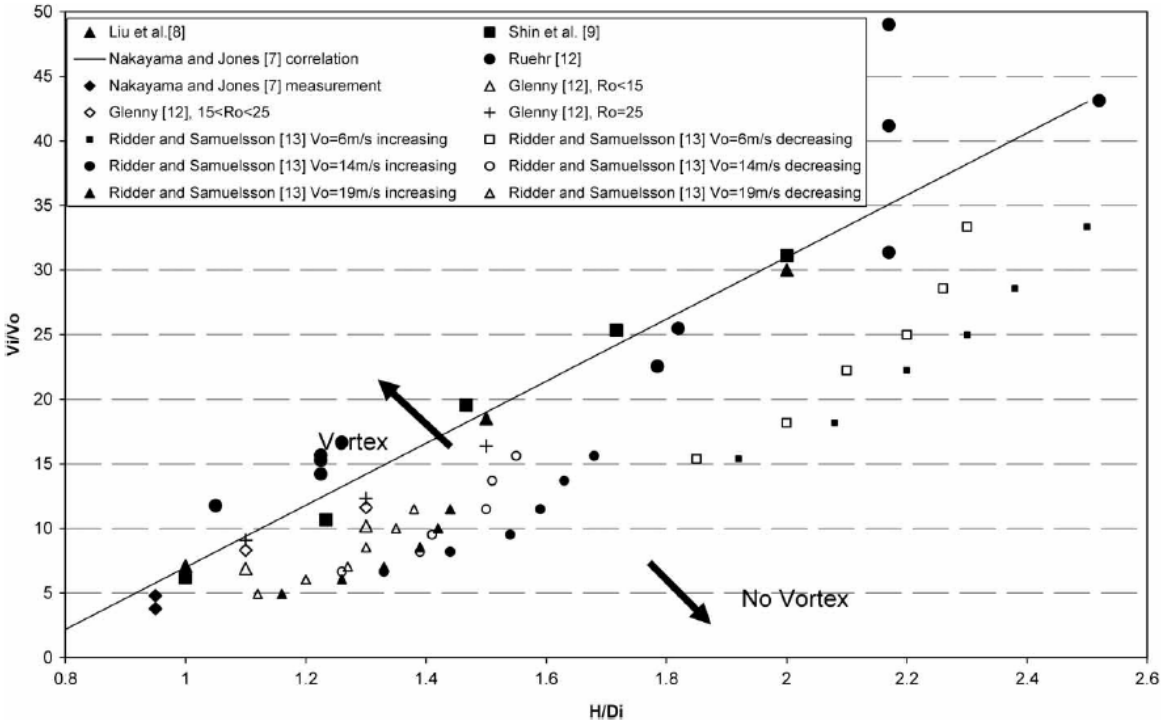

Figure 4: Experimental Data Displaying Vortex Formation Conditions [1]

The dividing line in Figure 4 does not always hold true due to hysteresis. The thresholds at which a vortex will form are different when the inlet velocity (V_i) is increasing than when decreasing. If the vortex has already formed and V_i is decreased the vortex may remained formed even when in the blow-away velocity conditions. In this research V_i was held at a steady-state value for each configuration.

1.1.2 Damage Caused by Vortex Formation

Damage can occur in multiple ways to the engine through the ingestion of a vortex, including lifting debris into the engine and potentially damaging the internal components. This is referred to as Foreign Object Damage (F.O.D.). As mentioned in Section 1.1.1, when the stream tube intersects the ground plane there is an induced ground flow. This induced ground flow will encompass debris which can eventually be ingested by the engine. The suction force of a vortex is larger than the average inlet suction of a jet engine without a formed vortex; thus, a vortex is able to pick up larger debris. According to Klein, the average suction force of a full scale jet engine without a vortex is less than one pound, however, an inlet vortex is able to generate 40 lbs of suction force [7]. The debris can lead to immediate engine damage by potentially destroying engine fan blades or causing blade erosion and dust deposits over time [3].

Two additional adverse effects of ingested vortices include causing vibrations of compressor or fan blades which may lead to structural fatigue over time, and compressor stall [1-3]. Compressor stall leads to a decrease in efficiency of the engine which implies more fuel being used during takeoff. It is also possible that if the resulting forcing function of the stall matches the compressor blade vibrational frequency then the stresses felt will be large and can cause blade fatigue failure. This can result in the entire blade row being destroyed [8].

1.1.3 Previous Research Techniques

Due to the damaging effects of these vortices on jet engines, research with vortex formation has been conducted since 1955 [9]. According to Trapp, research was first conducted using full scale engine facilities, however, this allows the possibility of jet engines being destroyed as shown in reference [3, 10]. This path of research can be rather expensive, leading to the development of engine simulators to help reduce the cost of jet engine testing while studying the effects of vortices [3].

To ensure safe and efficient jet engine designs, engine simulators are used in analyzing the flow qualities and performance of the jet engine. The engine simulators are scaled models of actual jet engines and can be either ejector-driven or driven by turbines. An ejector-driven simulator has interior nozzles that eject compressed air in order to drive the flow of the engine while turbine-driven simulators have moving blades to move the air flow. Inlet distortion is one common metric for defining the flow quality in the inlet of a jet engine. Inlet distortion is the measure of the overall changes of pressure over the inlet plane. Ejector-powered simulators provide a platform on which experiments can be performed under high bellmouth distortion conditions without damage to the simulator because there are no moving parts. This allows analysis of the flow under conditions that would likely damage an actual jet engine. These ejector-driven engine simulators have been successfully applied to aerodynamic studies carried out at the Aeronautical and Astronautical Research Laboratories, AARL [10, 11].

Even with the all the benefits of using engine simulators, there are some physical limitations in scaled testing, specifically with pressures and temperatures measurement

locations. Researchers are always searching for ways to increase modeling flexibility, and to decrease project time and costs. Modeling engine flow through computational tools has been under development since the 1970s, and has been recently implemented to study vortex formation [2, 3].

Computational Fluid Dynamics (CFD) is another useful tool for analyzing fluid flow. CFD is a tool that can be used to build a computational environment capable of analyzing the fluid flow around various objects, and provides the capability of determining the interactions between the fluids and surfaces in these given computational environments. CFD programs are governed by conservation of energy, mass, and momentum equations which allow for the varied use of the CFD programs.

The implementation of a CFD analysis tool allows one to design and analyze a new system or analyze a pre-existing system. CFD also provides the possibility for flow analysis in areas of flow that have been difficult to examine experimentally. An object to be analyzed in CFD is first modeled in a Computer-Aided Design (CAD) program, such as SolidWorks or ANSA, and then imported into a CFD program. Both SolidWorks and ANSA were used in this research, and ANSYS Fluent, a CFD program, was implemented to study the inlet flow conditions of a jet engine simulator.

1.1.4 Vortex Prevention Methods

Methods for preventing F.O.D. have been under research alongside the increasing developments made with jet engines. The best method may at first seem to be to raise the engine centerline height until the stream tube does not induce a ground flow, however, due to the physical constraints of aircraft sizes, this is generally not a feasible option. Different mechanisms have been developed for aircraft that would prevent F.O.D, with the goal to prevent relying upon airport runway cleaning due to the high cost and low efficiencies of this process. The development of such a prevention method might also allow jet engine aircrafts to operate on unpaved runways [3].

These mechanisms usually tried to prevent a vortex from forming due to the large suction force that resulted from a formed vortex. The first system implemented was developed by Harold J. Klein and was implemented on the DC-8 aircraft in the late 1950s [7]. He created a single jet system that would push a jet of air toward the vortex stagnation area as shown in Figure 5. The jets of air would increase the ambient velocity locally and thus make the conditions such that the blow-away velocity, as described in 1.1.1, was reached. However, this system was limited based on vortex formation outside of its operating conditions where the stagnation point of a vortex can move and thus be difficult to be targeted by jet flow. The jet also was known to impinge on debris and project them up, increasing their chances of being ingested into the inlet.

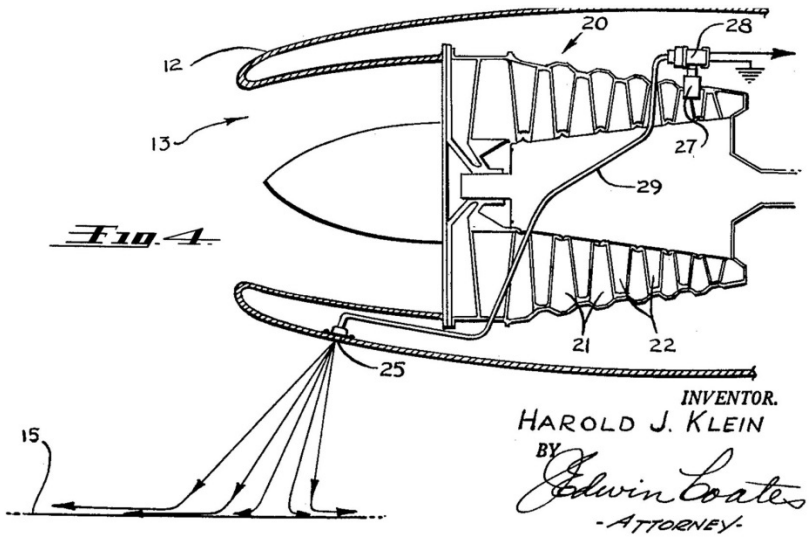

Figure 5: Klein Single Jet Prevention Invention [7]

Other techniques have been developed that include both active and passive prevention methods. One example of a passive prevention method is the inlet-vortex attachment developed by Cox and William shown in Figure 6. This system would deploy a panel between the bottom of the inlet and the ground plane. The idea was to provide a debris free surface for which the vortex could form, preventing F.O.D. However, in most instances the vortex would form around the panel as in Figure 6. In any case, a vortex still formed and could damage the engine.

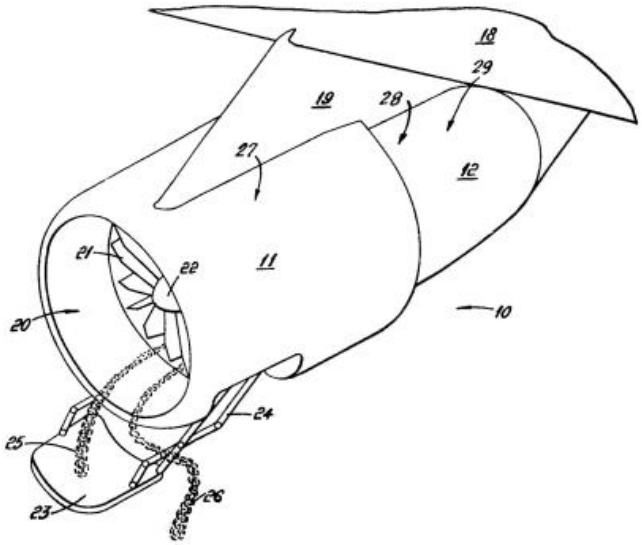

Figure 6: Cox and William inlet-vortex attachment [3]

Despite the range of prevention systems that exist, there is still much room for improvement. The methods described had the potential to increase the drag of the aircraft, bleed large amounts of air from the engine, which decreases engine efficiency, and actually cause debris to be ingested by the engine [3, 8]. However, a system is still desired that will prevent the formation of a vortex while having limited negative aerodynamic effects on the aircraft. More research is still needed to obtain a better understanding of the fundamentals of vortex formation.

1.2 Purpose of Current Research

The present research seeks to create a CAD model of an engine simulator in its environment and implement an existing CFD program to analyze the inlet flow of the modeled jet engine simulator. This tool will be designed to study the flow at various

conditions that have the potential to produce vortex formation. This computational environment will be constructed using an existing jet engine simulator experimentally developed test results as a verification and validation tool for the CFD results. The CFD environment will provide a tool to better understand vortex formation induced by jet engines when in taxiway operations. This tool will also provide a foundation to build upon the use of computational modeling in jet engine test simulation testing.

Three variables, each at three different conditions, will be analyzed in this research. The inlet mass flow will be set at values corresponding to full, cruise, and idle thrust of the engine simulator. The centerline height of the full scale engine will be modeled for 36.3 ft, 20 ft, and 9.5 ft. Considerations for choosing these centerline heights are discussed in Chapter 2. The different mass flow and centerline height settings will be tested under no crosswind conditions, five mph headwinds, and five mph crosswinds at 90° to the inlet. These conditions are also described in more detail in Chapter 2.

Chapter 2: Experimental Apparatus

2.1 Experimental Facility Description

All experimental work was performed at the Aeronautical and Astronautical Research Laboratories. This research laboratory is located by the Don Scott Airport, northwest of The Ohio State University main campus. The facility supports a high pressure air supply system which was used for running the engine simulator in this experiment.

2.2 Engine Simulator

In order to properly model a full scale jet engine, three main parameters must be met: first, the physical shape of the scale model must correctly match the full scale engine, second, the bellmouth flow of the model must match the full scale for all thrust settings, and third, the engine simulator must properly match the exhaust flow [10, 11]. All three parameters have been shown to correctly match full scale results in previous studies [10, 11]. The physical shape and engine inlet flow of the engine simulator were of primary concern in this study.

An existing engine simulator was utilized for this research. The engine is a 1:12 scale, ejector-powered simulator (EPS). The ejectors are placed circumferentially inside the engine in order to achieve uniform exhaust flow[11]. The ejectors push air through the engine which induces a lower pressure within the engine and results in air being pulled in through the inlet. These ejectors are powered by three air supply lines which are connected to the two high pressure air storage tanks capable of holding approximately 1500 cf at 2500 psig. The desired inlet flow is obtained by setting the drive pressure for each of the three air supply lines.

2.3 Experimental Setups

An outdoor “free field” facility provides a near-ideal environment for measuring the baseline conditions of an engine, Figure 7. In an ideal free field configuration, no ground plane would be present. Notice this is impossible to be completed experimentally, it is easily accomplished computationally. The engine centerline height was desired to be as far above the ground plane as possible to avoid ground effects on the engine performance. When the engine is tested on a stand outdoors under a no-wind condition, only the required air is drawn into the engine, and the thrust measured is the true thrust, aerodynamically require thrust, of the engine. The results obtained on a free field stand will provide the baseline information used in the investigation [10, 11]. A free field stand was used for this experiment. However, the engine centerline height was varied to study the ground effects. Three centerline heights were tested for this experiment: free field

(36.3”), 20 inches, and 9.5 inches with a tolerance of ± 0.0625 of an inch for each setting. These centerline heights correspond to the full scale engine heights.

2.3.1 Free Field Stand

The free field stand implemented in this study is shown in Figure 7. Construction details can be found in reference [11]. The engine centerline height for this configuration was set to 36.3 inches. This was the center most position the engine could be placed within the connecting strut to the free field stand. A center position was set to minimize any flow separation caused by the support beams.

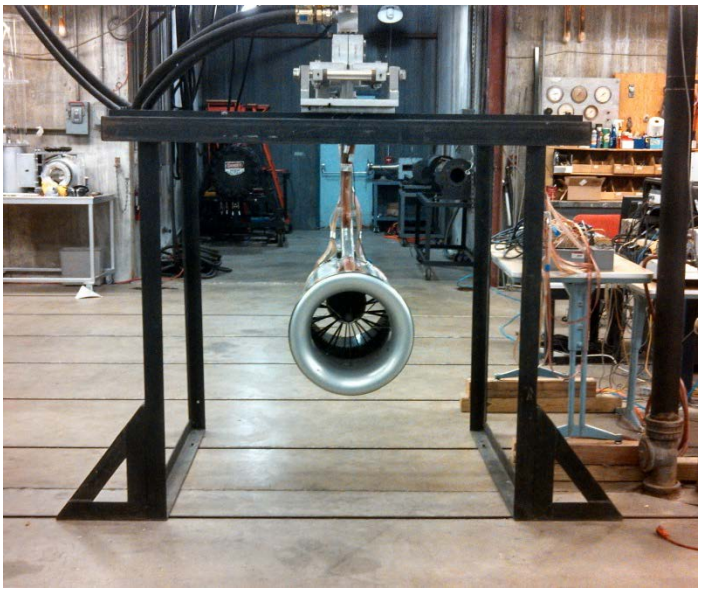

Figure 7: Free Field Stand

As discussed in Chapter 1, each of the three centerline heights was tested with and without crosswind conditions. A five mph crosswind was provided using an industrial sized flow. The effects of swirl, circular rotation, due to the fan were considered negligible, and the flow was treated as uniform in this research. The two crosswind

configurations included: 0°, or known as a headwind, and 90° as shown in Figure 8 and Figure 9, respectively. In order to make the fan flow as uniform as possible at the engine inlet, the fan was placed on a table which aligned the fan centerline with the engine centerline. The table was placed eight feet from the engine centerline which allowed the fan flow to decrease to a five mph velocity. This distance also allowed the fan to be out of the area affected by the engine inlet, which will be discussed in more detail in Section 2.3.2. The same crosswind configuration was tested for the other centerline heights.

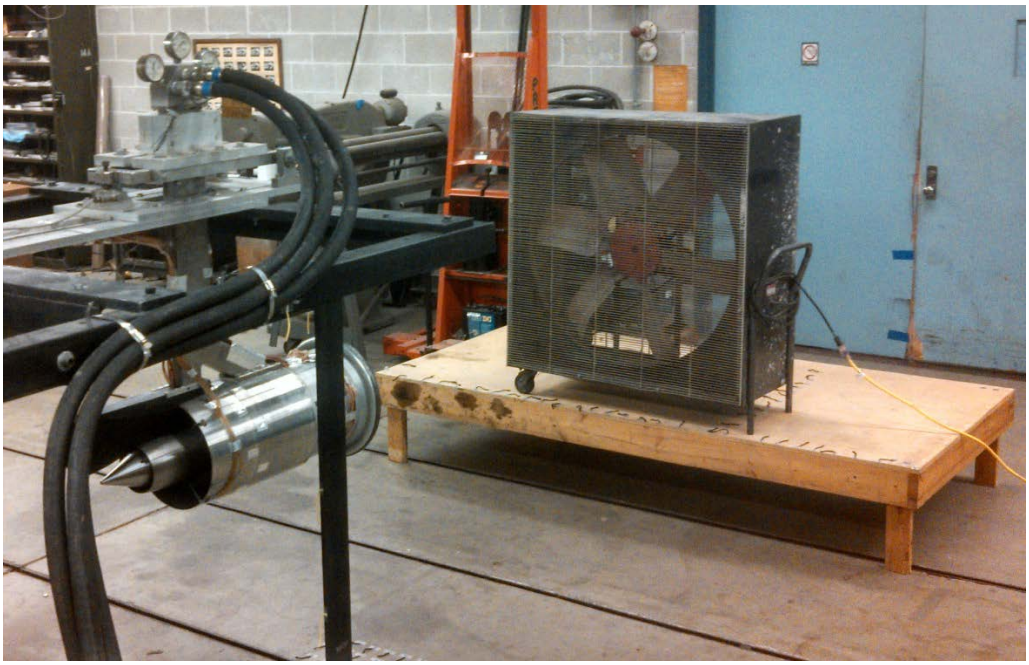

Figure 8: 0° Headwind for Free Field Configuration

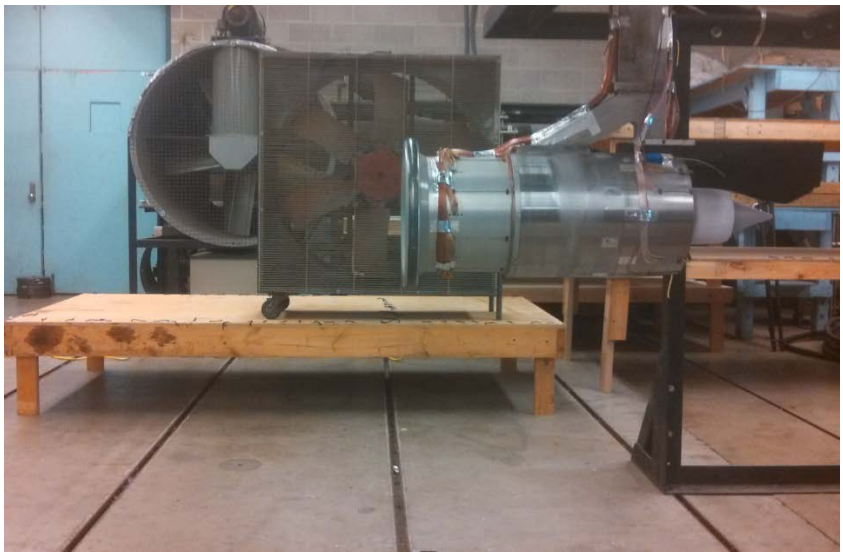

Figure 9: 90° Crosswind for Free Field Configuration

2.3.2 Engine Test Stand

The 20 inch centerline height was selected to simulate a typical engine manufacture free field stand. For example, GE Aviation has a 20 foot, single post, free field jet engine test stand. The free field stand used at the AARL was not capable of lowering the engine to a 20 inch to a 9.5 inch centerline height. Tables were made from 4'x8' particle boards to achieve the desired centerline height, Figure 10. The tables were sanded to create a smooth surface. Any holes located on the tables were taped over to prevent flow separation or turbulence. From the front of the engine, the tables extended eight feet on both sides and eight feet forward. Figure 10 shows that tufts were placed around the edges of the tables to visualize the airflow. The tufts were observed to be nearly stagnant at the edges of the tables at all thrust settings which implied that was minimal flow separation from the edge of the table affecting the engine performance.

Figure 10: 20" Centerline Height Experimental Setup

The Boeing 777-300ER [12] GE90 engine centerline height is shown in Figure 11 to be slightly below Height C. By referencing Table 1 Height C is shown to be between 9.2 inches and 10.2 inches. Therefore, the centerline height of the engine was estimated to be 9.5 inches for ease of measurements. The engine simulator was placed at a 9.5 inch centerline to simulate the full scale engine over the tarmac. The flow seen by the engine simulator test cell bellmouth and the full scale engine with flight cowl on the Boeing 777-300ER will not be the same. However, this centerline height was used as a baseline to determine the general conditions at which a vortex would form for this engine. A flight cowl was not available for the existing engine simulator.

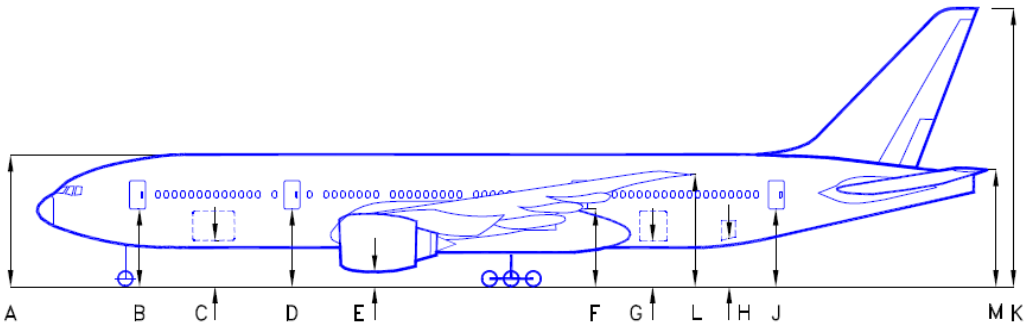

Figure 11: Boeing 777-300ER [12]

Table 1: Boeing 777-300ER Heights[12]

	MINIMUM*		MAXIMUM*	
	FT - INCHES	METERS	FT - INCHES	METERS
A	27 - 5	8.36	28 - 7	8.70
B	15 - 5	4.69	16 - 7	5.06
C	9 - 2	2.79	10 - 2	3.11
D	15 - 11	4.85	16 - 10	5.11
E	2 - 4	0.70	2 - 10	0.88
F	16 - 10	5.14	17 - 5	5.30
G(LARGE/SMALL DOOR)	10 - 6	3.19	11 - 9	3.58
H	11 - 2	3.40	11 - 10	3.61
J	17 - 5	5.31	18 - 1	5.52
K	60 - 8	18.48	61 - 6	18.75
L	23 - 6	7.16	24 - 7	7.49
M	26 – 2	8.06	27 – 5	8.34

Figure 12: 9.5" Centerline Height Experimental Setup

2.4 Instrumentation

In this section, the different instrumentations used during experimental testing will be described, including pressure and temperature data collection. All data collected was compiled by the lab computer and printed out in a lab specific format.

2.4.1 Pressures

The engine simulator was connected to a vertical air supply strut that allowed the connection of the engine to the free field stand and the three air supply lines, Figure 13. These lines were connected to a control system shown in Figure 14 . Each valve for the air supply is operated manually and is monitored by a pressure gauge, and each air supply is capable of providing the engine up to 2000 psig of high pressure air.

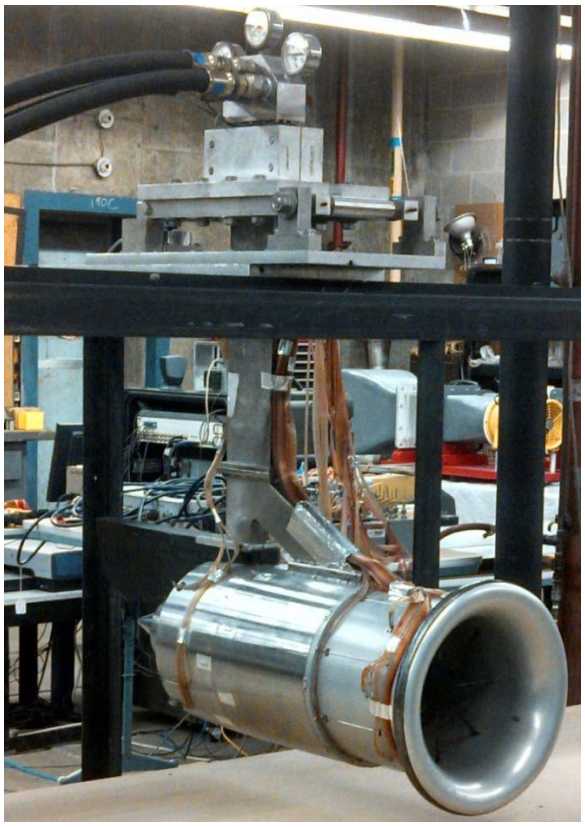

Figure 13: Engine Connected to Vertical Strut

Figure 14: Air Supply Control System

To import the drive pressures to a computer readout, a Validyne Carrier Demodulator signal conditioning unit (CD-15) is used. A differential pressure transducer, Model DP-15, measured the drive pressure and output a signal to the CD-15, which in turn delivered the data to the computer. For more information on the DP-15 and CD-15 refer to references [13] and [14], respectively. The ambient pressure was measured using a standard pressure barometer.

There were two types of pressure monitors in the engine simulator. Both total pressure probes and static pressure taps are located throughout the engine at various engine measurement planes. The engine bellmouth is designated Plane 7, and instrumented with eight pressure rakes each consisting of five total pressure probes (see Figure 15). In order to obtain distortion at the plane, the eight rakes were equally spaced radially, with each of the five probes located at the center of rings of equal areas as shown in Figure 16 [15]. There are eight static pressure taps located between the total pressure rakes on the engine simulator interior wall, also equally spaced.

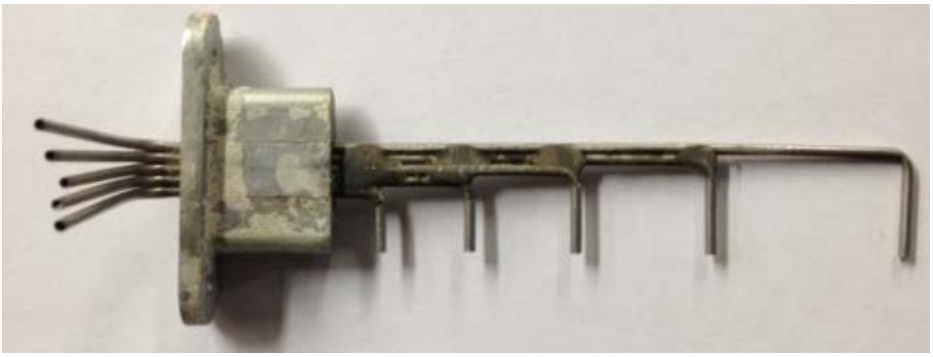

Figure 15: Total Pressure Rake

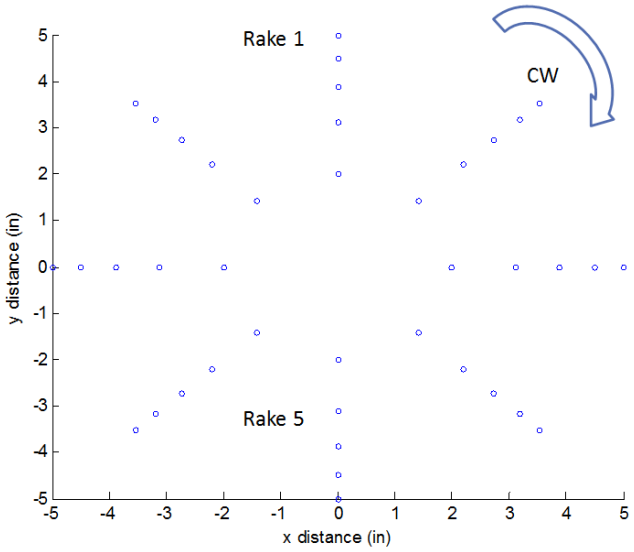

Figure 16: Aft Looking Forward, Plane 7 Total Pressure Probe Locations

The pressure probes and taps are connected to 1/8” outer diameter plastic tubing. This tubing runs from the engine simulator to the Pressure Systems INC pressure modules, equipped with 16 pressure transducers that are connected to the rubber tubing by use of the 1/8” metal tubes as shown in, Figure 17.

Figure 17: Pressure Bricks

One psi pressure transducers were used in the modules connected to Plane 7. These were used in order to gain the highest possible accurate reading available in the bellmouth plane. According to reference [16], the one psi transducers are rated to have a ±0.15 % full scale (FS) accuracy. This corresponds to measurement accuracy of ±0.0015 psi or ±0.042 inH20.

2.4.2 Temperatures

Temperature measurements were gathered using Type T Quick Disconnect Thermocouples made by Omega, shown in Figure 18.

Figure 18: Thermocouples

These thermocouples have a an accuracy of ±1.8 °F [17]. A total of five thermocouples were used during testing. One thermocouple measured ambient temperature, three thermocouples were used to measure the temperatures of the air in each of the three air supply lines, and the fifth thermocouple was attached to the exhaust plane of the engine to measure the temperature of the engine exhaust flow.

Chapter 3: Test Procedures

Data from the experimental runs performed were collected and evaluated by the laboratory's computer. A LabVIEW program organizes the data and evaluates the results to calculate desired parameters. This program was created by Aerodyne Research Incorporated which converted an existing AARL FORTRAN-based software system to LabVIEW.

3.1 Experimental Procedures

This section discusses experimental methods and procedures. First, the physical parameters of the engine are inputted into the computer, which include: centerline height, number and location of the pressure probes, reference temperatures, and engine dimensions. With these parameters defined the CD-15s were calibrated. Then pressure bricks shown in Figure 17 would be calibrated. The calibration allowed the pressure bricks to reset the transducers to the test day ambient pressure conditions. Upon completion of the calibrations, the computer is ready to take data and the run can begin. An operator will turn the valves at the monitoring station shown in Figure 14, and the drive pressures are verified through a real-time drive pressure display on the computer.

Once the desired pressure was reached, the computer operator will begin the recording, which samples data over five seconds and averages the results. The provided data includes the pressures at all the engine simulator probe locations, inlet velocity, bellmouth distortion, and engine thrust. In this research the main parameters of concern were the inlet velocity, inlet mass flow, and bellmouth total pressure distortion.

3.2 Reduced Data Definitions

During scale model testing, one of the important parameters analyzed is bellmouth distortion. This is an industry-established indicator of airflow quality. The pressures at Plane 7, as defined in Section 2.4.1, are used to calculate the bellmouth distortion, BM_{Dist}, which is defined as follows:

$$BM_{Dist} = \frac{P_{max} - P_{min}}{P_{avg}} * 100\% \quad (1)$$

Where P_{max} is the maximum pressure, P_{min} is the minimum pressure, and P_{avg} is the average pressure at Plane 7.

As discussed in Section 1.1.1, the pressure in a vortex is lowest in the core. To see the vortex in the bellmouth pressure readings, the core must align with one of the total pressure probes in Plane 7. Referring to previous works [1-3], the vortex is predicted to form somewhere in the vicinity of rakes 4-6, Figure 16. Thus, one of the pressure probes will display a lower pressure than the rest of the probes. This lower pressure will

noticeably increase the bellmouth distortion. The bellmouth distortions with vortex capture will be compared to those that have no vortex formation.

Chapter 4: Experimental Results

The experimental results will be discussed in two sections. First, the results with no crosswind will be discussed, followed by the results from both the headwind and 90° crosswind. These results will be compared to previous experimental results.

4.1 Ideal Conditions Results

In order for a vortex to form, either ambient vorticity or a crosswind must be present but low enough to be less than the blow-away threshold. In an ideal condition the ambient vorticity and crosswinds would be zero, and no vortices are expected to form. However, due to the need to evacuate the engine simulator exhaust from the building and allow sufficient airflow to the engine inlet, multiple doors were opened during testing. Based on physical constraints, the exhaust of the simulator was not able to be aligned with the exhaust door, which caused some recirculation in the testing room which caused both artificial crosswinds and ambient vorticity. It was understood that due to these conditions, and the low $\frac{H}{D}$ value for the 9.5 inch centerline, that a vortex could form.

The $\frac{H}{D}$ values tested are tabulated in Table 2. As stated under ideal conditions,, the crosswind value would be zero. The normalized heights were plotted against the ideal

normalized velocity values, shown in Figure 19. This figure uses the same correlation line and axis limits as Figure 4 for ease of comparison. All three conditions are in the no vortex forming region.

Table 2: Normalized Heights (H/D)

Free Field	3.83
20" Centerline	2.11
9.5" Centerline	1.0

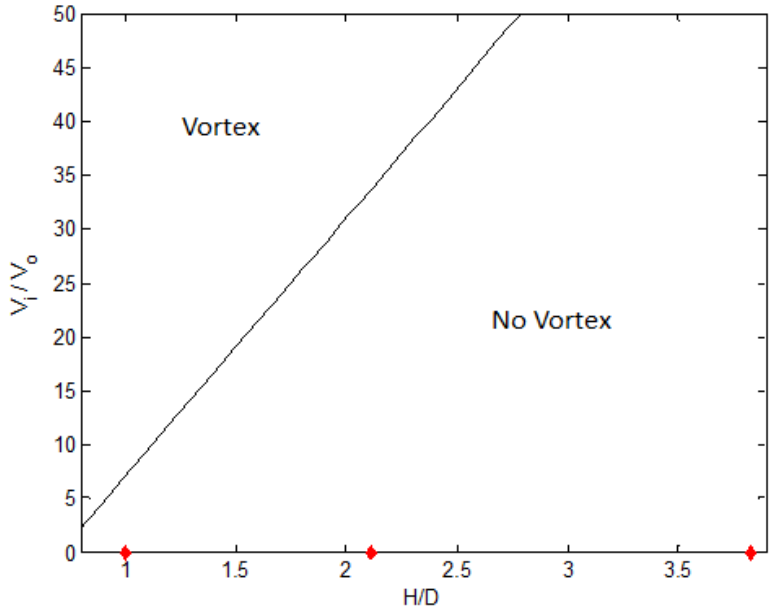

Figure 19: No Crosswind Ideal Conditions

Each height setting was tested at three different velocities, based on different thrust settings. Table 3 shows the correlation between the velocity nomenclature and the thrust settings. The average velocities and mass flows were calculated for each of the

three thrust settings and then tabulated in both SI and English units as displayed in Table 4. The velocities ranged ± 6 m/s from the averaged value.

Table 3: Thrust Setting Definitions

Nomenclature	Thrust Full Scale (lbs)
Idle	8,800
Cruise	33,000
Full	88,000

Table 4: Average Inlet Flow Values

	Mass Flow (kg/s)	Mass Flow (lbs/s)	Velocity(V_i) (m/s)	Velocity(V_i) (Ft./s)
Idle	3.27	7.2	58	190.3
Cruise	5.58	12.3	100	328.1
Full	7.70	17.0	151	495.4

The mass flow values were used in the CFD analysis and the velocities were used to compare the results. Originally the author desired to compare bellmouth distortions, however, this was not possible and will be discussed in further detail in Chapter 6.

Each configuration was run at least three times in order to gain a more accurate average value of inlet conditions. The average bellmouth distortion for each run was tabulated and is shown in Table 5. A vortex did form under a 9.5 inch centerline height at the full velocity setting, and the bellmouth distortion corresponding to the vortex formation run was not averaged in order to maintain the distortion index.

Table 5: Ideal Conditions-Average Bellmouth Distortions

Height	Velocity	Average BM Distortion (%)
Free Field	Idle	0.016
	Cruise	0.035
	Full	0.08
20"	Idle	0.013
	Cruise	0.05
	Full	0.066
9.5"	Idle	0.023
	Cruise	0.033
	Full	0.061

Total pressure distribution contour plots were created to visualize the pressure distortions at Plane 7. Figure 20 displays the total pressures for a free field, full velocity setting. As to be expected, the total pressures matched ambient pressure for the test day. Without vortex formation, the total pressure should be ambient pressure due to no work being done on the system. A sampling of total pressure plots for all 9 run configurations can be found in Appendix A.

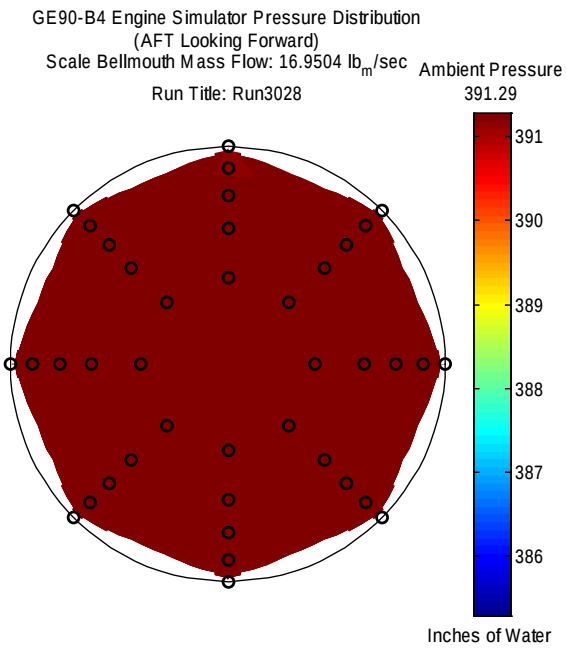

Figure 20: Free Field Total Pressure Plot at Full Velocity with no Vortex Capture

The pressure plot showing a vortex for the 9.5 inch, full velocity run is displayed in Figure 21.

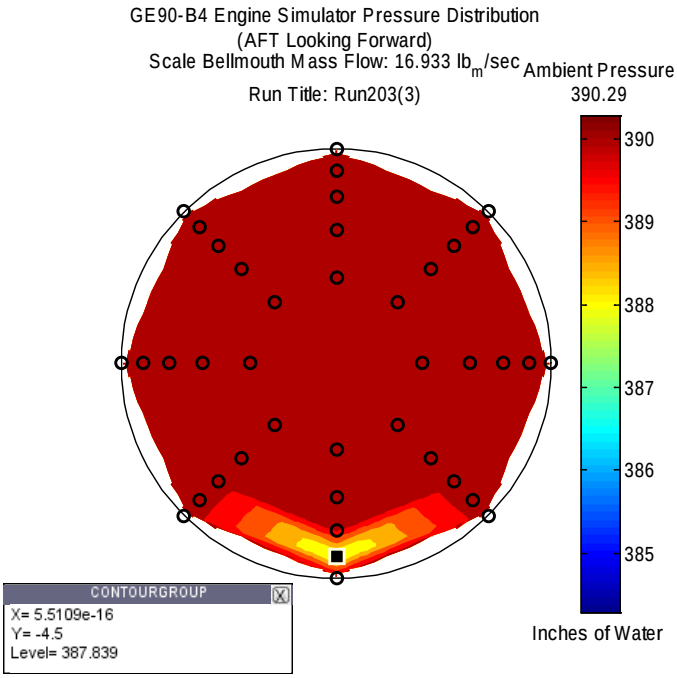

Figure 21: 9.5" Centerline Total Pressure Plot at Full Velocity with Vortex Capture

The bottom left of the figure shows the x and y coordinates as well as the total pressure at the probe. There was a distortion of 0.65% at the bellmouth, an increase of 0.59% compared to the runs without vortex capture. The difference in ambient pressure between Figure 20 and Figure 21 is due to the runs occurring on different test days.

4.2 Crosswind Conditions Results

Crosswinds were tested to determine the effects on bellmouth distortion. Five mph crosswinds were directed at the engine inlet at 0°, headwind, and 90° angles. The average velocities in Table 4 were normalized with respect to the 5mph, 2.2 m/s, crosswind, and the results are shown in Table 6. These values were plotted verses the

corresponding normalized heights listed in Table 2. The results along with the vortex correlation factor are shown in Figure 22.

Table 6: Normalized Velocities

Thrust Setting	(Vi/Vo)
Idle	25.95
Cruise	44.74
Full	67.56

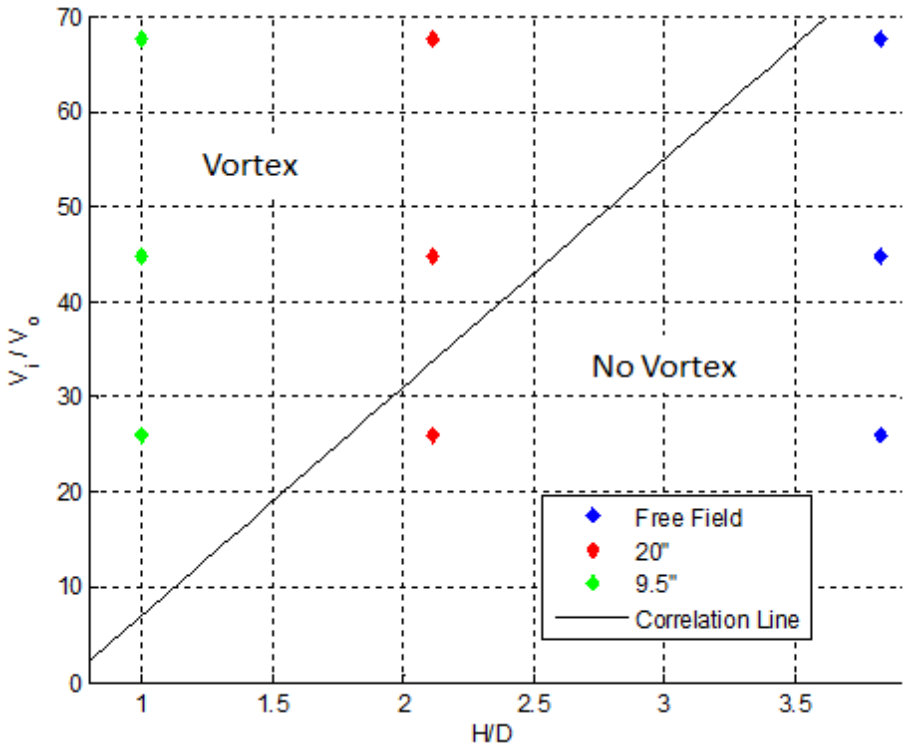

Figure 22: Experimental Configurations with Crosswind Plotted with Vortex Correlation Line

A vortex was predicted to form for all 9.5 inch centerline configurations and for the two higher thrust configurations for the 20 inch centerline. As discussed previously,

the location correlation line is not agreed upon, and that it is possible some of the settings could be in a different region of the plot if a different vortex correlation line was chosen.

The bellmouth distortion was averaged across multiple runs for each configuration, and each average is listed in Table 7. The averaged values did not include any runs that captured a vortex.

Table 7: Crosswind Configurations-Average Bellmouth Distortions

Height	Velocity	Crosswinds	Average BM Distortion (%)
Free Field	Cruise	0 Degree (Headwind)	0.073
		90 Degree	0.073
	Full	0 Degree (Headwind)	0.082
		90 Degree	0.065
20"	Idle	0 Degree (Headwind)	0.070
		90 Degree	0.056
	Cruise	0 Degree (Headwind)	0.070
		90 Degree	0.080
	Full	0 Degree (Headwind)	0.075
		90 Degree	0.080
9.5"	Idle	0 Degree (Headwind)	0.050
		90 Degree	0.050
	Cruise	0 Degree (Headwind)	0.090
		90 Degree	0.080
	Full	0 Degree (Headwind)	0.047
		90 Degree	0.065

Table 8 shows the distortion values summary for runs in which a vortex was successfully captured at the 9.5 inch centerline configuration. A sample of the total pressure plots are also provided in Figure 23 and Figure 24, with the remaining plots located in Appendix A.

Table 8: Vortex Formation Bellmouth Distortions

Height	Velocity	Crosswinds	BM Distortion (%)
9.5"	Idle	0 Degree (Headwind)	0.29
		90 Degree	0.54
	Cruise	0 Degree (Headwind)	0.15, 0.25
		90 Degree	3.47
	Full	0 Degree (Headwind)	0.22
		90 Degree	1.12

Figure 23 displays the results for a non-captured vortex run at cruise velocity with a 90° crosswind, where Figure 24 shows the results for the same run conditions, but with a captured vortex. The low pressure region can clearly be seen in rake five and is 13.2 inH20 lower than ambient pressure. This resulted in the largest bellmouth distortion of this research with a value of 3.47% which is extremely high by industry standards.

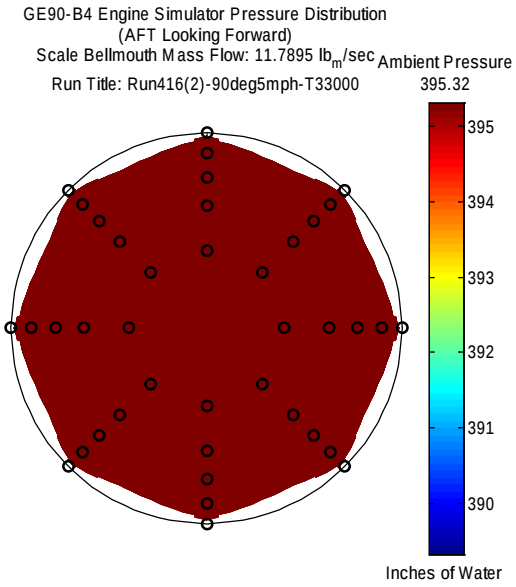

Figure 23: 9.5", 90° Crosswind, Cruise Velocity, No Vortex

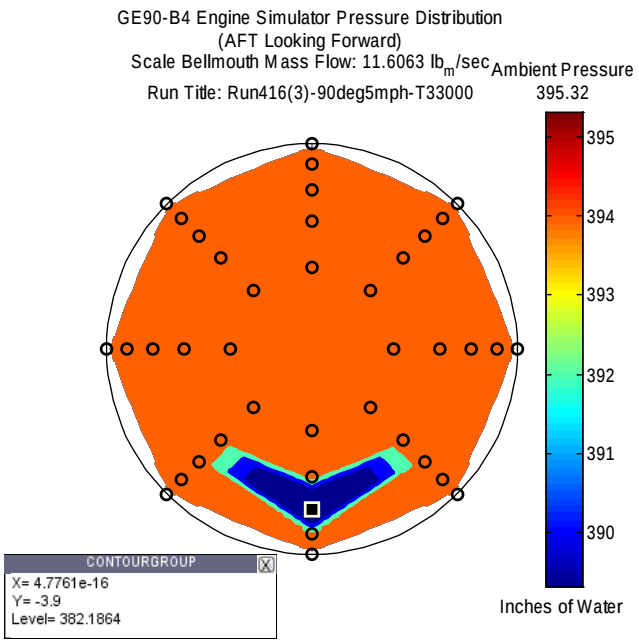

Figure 24: 9.5", 90° Crosswind, Cruise Velocity, Vortex Formation

Figure 25 and Figure 26 are the pressure plots for full velocity with 90° crosswind. These are comparable with Figure 20 and Figure 21, which were under the same conditions but with no crosswinds. The bellmouth distortion with crosswinds is much larger than without.

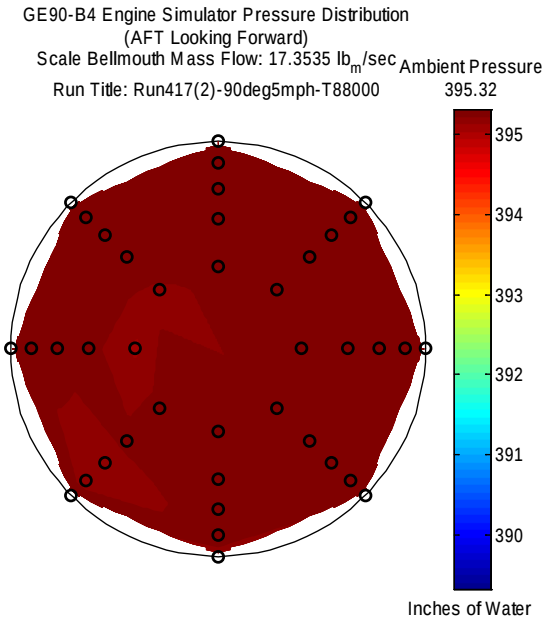

Figure 25: 9.5", 90 Crosswind, Full Velocity, No Vortex Capture

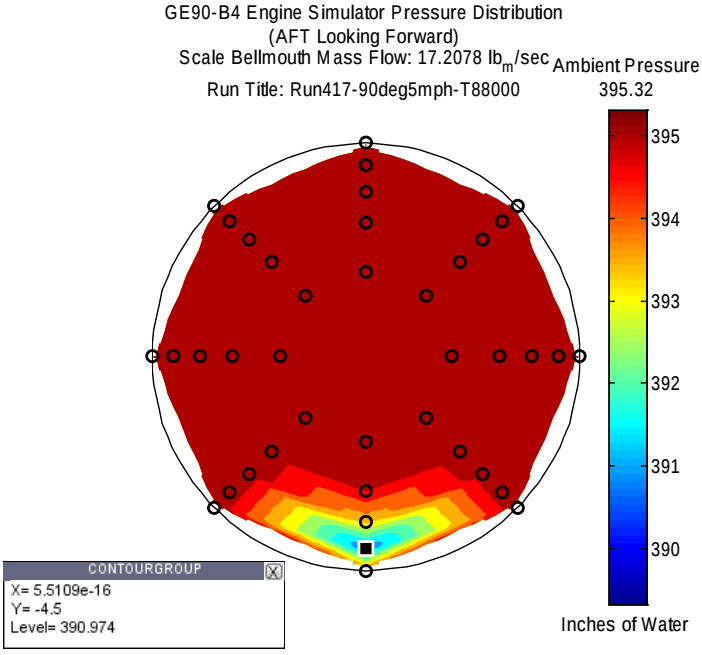

Figure 26: 9.5", 90 Crosswind, Full Velocity, With Vortex Capture

No vortices were captured in the 20 inch centerline configurations. One explanation could be due to the small size of the vortex core that enters the inlet, and may not have been captured by the probe. Another possible explanation is that the flow circulation in the lab was high enough that the vortex was unable to form.

Smoke and tufts were used to visualize the flow field near the engine inlet. The tufts were placed on the table below the engine. When a vortex formed the tufts were seen to rotate in a circular pattern and the vortex was seen to move around the table. The smoke was seen to swirl into the engine when it was caught in a vortex. The visualization tools showed vortex formation for all 9.5 inch centerline height conditions. Figures displaying both tuft and smoke results are located in Appendix A.

Chapter 5: Computational Modeling

CFD has been in existence since the 1950s. However, recent advances in computational systems have allowed this field to expand. CFD is becoming more prevalent within industry and government research facilities [18]. One common CFD programming tool is Fluent. This program has been implemented in many industrial and academic applications. Fluent has been shown to match experimental results; Fluent V14.0 was used in this research.

5.1 Producing a CFD Solution

Before implementing Fluent, the engine simulator first had to be modeled in a CAD program. The engine bellmouth was modeled using SolidWorks. The solid model was then imported into ANSA 13.2.1 for creating the computational domain and generating a numerical mesh for solving the governing equations.

The ceiling, floor, and side walls were all 8 ft from the engine centerline, and was chosen based on the discussion in Section 2.3.1. The engine exhaust was extended approximately 8 ft aft to allow enough room for the air flow coming through the domain from aft of the engine bellmouth location to completely develop, and not experience any

interference; placing the aft wall nine feet from the engine bellmouth. The forward wall was extended to 12 ft in front of the bellmouth to ensure that the flow was completely developed.

The domain was divided into four volumes to allow the generation of different coarseness of mesh. The mesh generation for each volume will be discussed in more detail in Section 5.1.1. The volumes were separated by interior planes, which are invisible to the flow and only serve as a function for mesh generation. The computational domain is labeled and displayed in Figure 27.

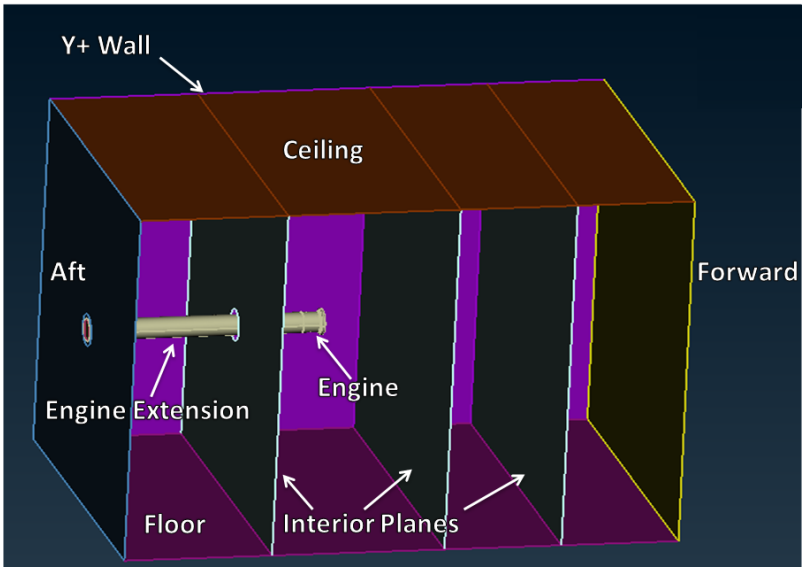

Figure 27: Computational Domain

The engine was divided into two volumes, with the interior of the extended exhaust tube set as a separate volume. This was done so that computational time was not used on modeling the flow in the tube, since this was not an area of study. The interior of

the actual engine model and the surrounding area up to 0.2 meters away was a volume with a very fine mesh surrounding the engine so that the flow coming into the engine would have high resolution.

Four boundary conditions (BC) were used to define the domain planes: Interior, P-inlet, Velocity Inlet, and a wall. The interior planes, as mentioned, allowed a plane to not be detected by the flow. A P-inlet, or Pressure Inlet, is used for flow inlets when the inlet flow is unknown, but the pressure is known. A velocity inlet boundary allows the velocity of a fluid to be set at a flow inlet, and the wall boundary condition sets the plane to interact with the fluid as a solid wall [19]. The pressure outlets for all configurations were set to standard day pressures, 0 psi gauge pressure. This was possible because all the experimental data is converted to standard day values. When the velocity inlet BC was used, the value was set at 5 mph in the direction depending on the run configuration. The wall BC was only used for the engine and the floor. Furthermore, the floor was only set as a wall in the non-free field configurations and as a P-inlet in the free field simulation in order to create the ideal configuration. Table 9 lists the planes and their corresponding boundary condition designations. These were changed depending on the run conditions.

Table 9: Domain Boundary Conditions

Plane Designation	Boundary Condition
Interior Planes	Interior
Ceiling	P-inlet
Floor	P-inlet, Wall
Y+ Wall	P-inlet
Y- Wall	P-inlet, Velocity Inlet
Forward	P-inlet, Velocity Inlet
Aft	P-inlet

5.1.1 Mesh Generation

The mesh was generated using ANSA. First a surface mesh was created on each of the planes using a triangular mesh, because this surface mesh is known to solve computationally faster than a square surface mesh. The volume mesh was then created off of this surface mesh. The large volume surrounding the engine had a mesh size of 0.40 mm for all configurations. The cylindrical volume surrounding the engine had a finer mesh size of 0.20 mm, generated in order to provide more detail in the flow solution. The rest of the volumes were coarsely meshed. The flow velocity in the remaining volumes was low enough that a coarse mesh allowed the flow to be solved to a high enough resolution while not demanding too much computational time. An example of a generated mesh is displayed in Figure 28. This is the mesh for the 9.5 inch centerline and has 7.77 million cells.

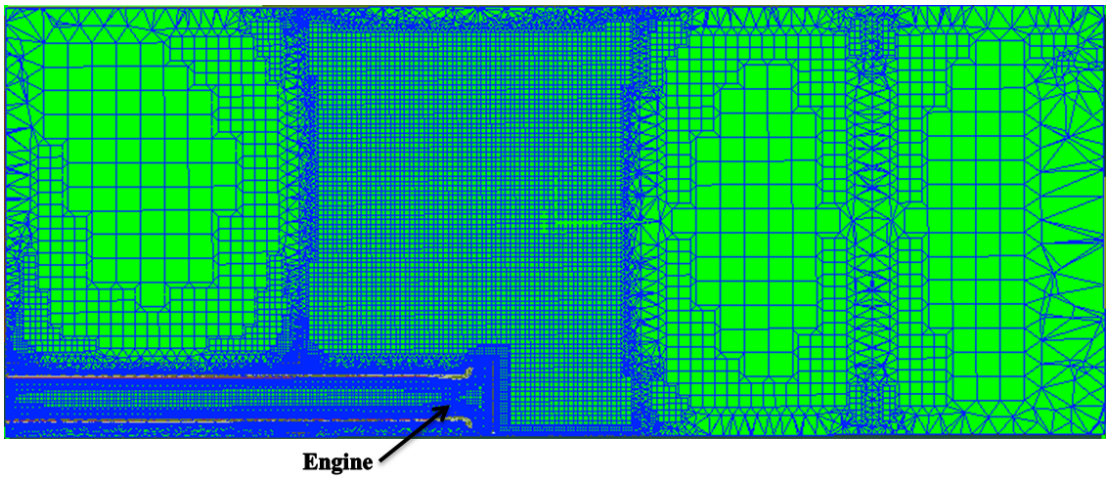

Figure 28: Example of Generated Mesh

5.2 Turbulence Modeling

Reynolds Stress Model (RSM) is a proper model to use for complex and rotating flow fields. Thus, the RSM would be a good modeler for this research. The model was implemented for the free field flow conditions. However, the computational time to solve a small number of iterations was too long and was unfavorable due to the extreme computational time.

The vortex formation at the engine inlet can be model using a steady-state modeler, however, a transient modeler is usually preferable to gain a more thorough understanding of the flow field. The author looked into implementing a transient model. The Courant number, described in Reference [18], was applied to the computational model and a time step of 0.000132 seconds was determined to be needed to accurately solve the flow. This resulted in the need for 320 time steps. Assuming the default of 20 iterations per time step, a total of 6400 iterations would be needed for one flow through

the computational domain. Usually, several passes are desired for model convergence. Assuming a minimum of 3 passes through the domain, a total of 19,200 iterations would be necessary; more if the flow did not converge. An iteration was observed to take an average of 1 minute to solve, which would require an estimated 13 days to solve one configuration with the available computational power. This was deemed too computationally expensive, resulting in a steady solver being implemented for this research.

5.2.1 Shear Stress Transport k-ω Model

The shear-stress transport (SST) k-ω was used because it is a robust model for solving near-wall region and far field flows. This model combines the near wall equations from the k-ω and the free field equations of the k-ε, and has been successfully implemented by Ho [1, 2, 6] to qualitatively show vortex formation.

There are two solvers that are used for solving the energy, continuity, and momentum equations: Pressure-based and density based solvers. The pressure-based solver is traditionally used to solve incompressible flows. It can also be used to solve mildly compressible flows, up to 0.7 Mach, with some accuracy. The density-based solver was designed for high-speed compressible flows. This solver has greater accuracy in high Mach numbers [19], but at a cost of being more computationally expensive. The free field, full mass flow, no crosswind configuration was run for over 20,000 iterations and the solution was still over 100 m/s from the experimental results, leading to the pressure-based solver as the chosen option for this research.

Chapter 6: Computational Results

Due to large domain building and computing time, a limited number of configurations were able to be investigated. Table 10 shows the original test matrix that was completed experimentally, the boxes marked are the runs that were computationally simulated.

Table 10: Completed CFD Simulations

Height	**Thrust**	**Crosswind angles**		
		0°	90°	None
Free Field	Full	*	*	*
	Cruise	*	*	*
	Idle			
20"	Full			
	Cruise			
	Idle			
9.5"	Full	*	*	
	Cruise			
	Idle			

The free field condition simulation was completed before trying the other centerline heights. Since there would be no vortex formation in free field conditions the convergence to a solution was more efficient. Upon successful completion of the free field, full mass flow simulation, investigation into the other centerline height simulations

began. First, this chapter will discuss the free field results and the challenges that emerged. Second, the complications with the 20 inch centerline will be overviewed. Third, the 9.5 inch centerline height results will be reviewed.

6.1 Free Field Results

Free field conditions were successfully simulated for both the full (17.0 lbs/s) and cruise (12.3 lbs/s) mass flow conditions. Due to limited availability of computational time on the Ohio Super Computer (OSC), the idle mass flow conditions were not able to be run for a sufficient number of iterations that would converge to a solution.

6.1.1 No Crosswind Conditions

The free field was first run at full mass flow setting with no crosswind. Figure 29 shows the velocity streamlines on the vertical cross-sectional xz plane. The streamlines start from the pressure inlets and are ingested into the engine, an expected behavior in free field conditions. The velocity contours near the engine bellmouth were plotted on the xz plane and are shown in Figure 30. The black box on the figure shows where the total pressure probes in the engine simulator correspond to the CAD model. The average velocity at the inlet was calculated to be 145 m/s. This value is in the range of velocities described in Section 4.1, closely matching the experimental results.

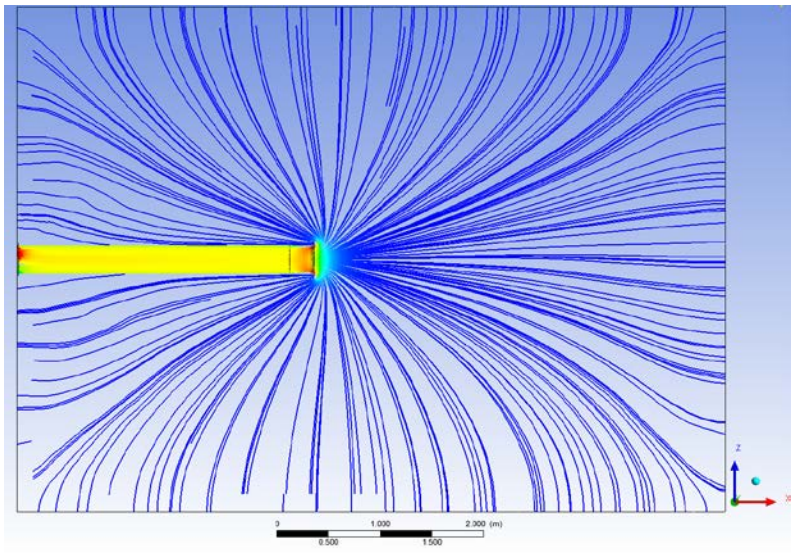

Figure 29: Free Field, Full Velocity, No Crosswind

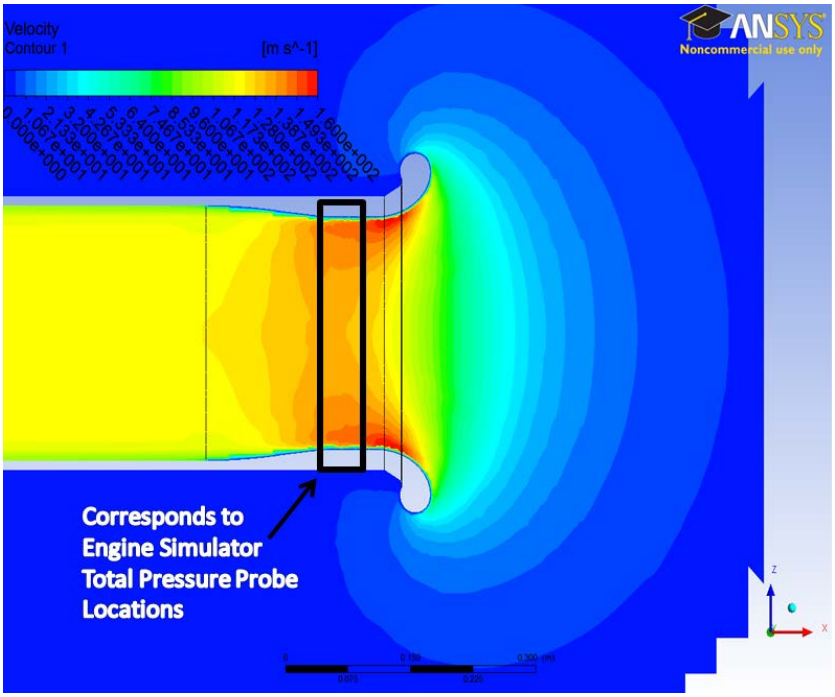

Figure 30: Free Field, Full Mass Flow, No Crosswinds, Velocity Contour

This configuration was also simulated at cruise mass flow conditions. The streamlines followed the same behavior as full mass flow conditions and is shown in Appendix B for direct comparisons with the full flow, the velocity contour plot at cruise conditions is located in Figure 31. The average velocity value was estimated at 100 m/s, corresponding to experimental results.

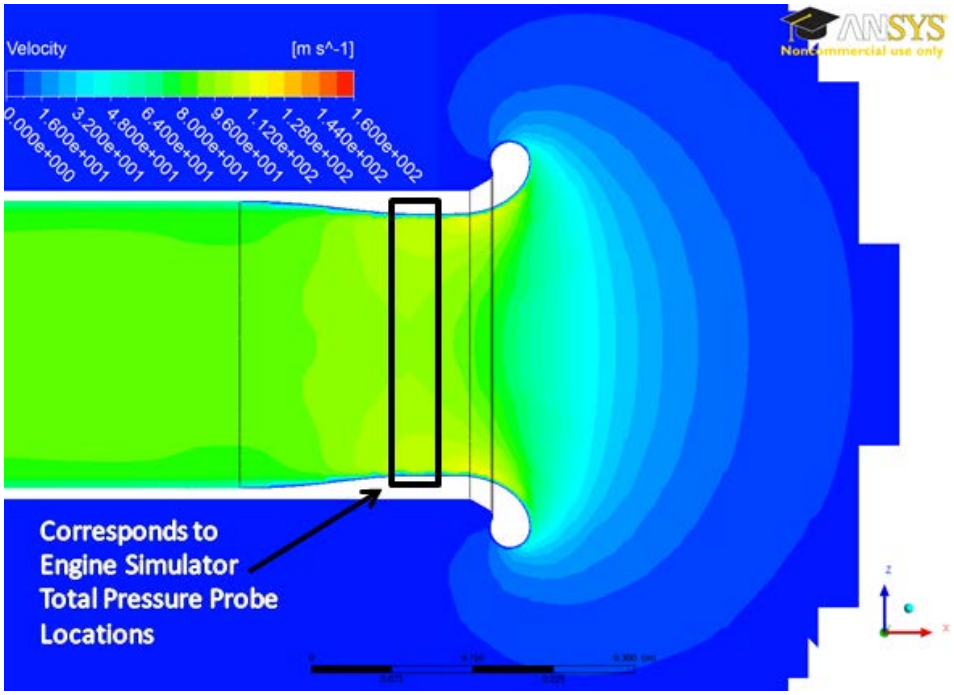

Figure 31: Free Field, Cruise Mass Flow, No Crosswinds, Velocity Contour

6.1.2 Crosswind Conditions

Crosswinds were next added due to the successful simulation of free field, no crosswind conditions. The velocity streamlines, plotted on the horizontal xy plane, for the 90° crosswind conditions and headwind are shown in Figure 32 and Figure 33 , respectively.

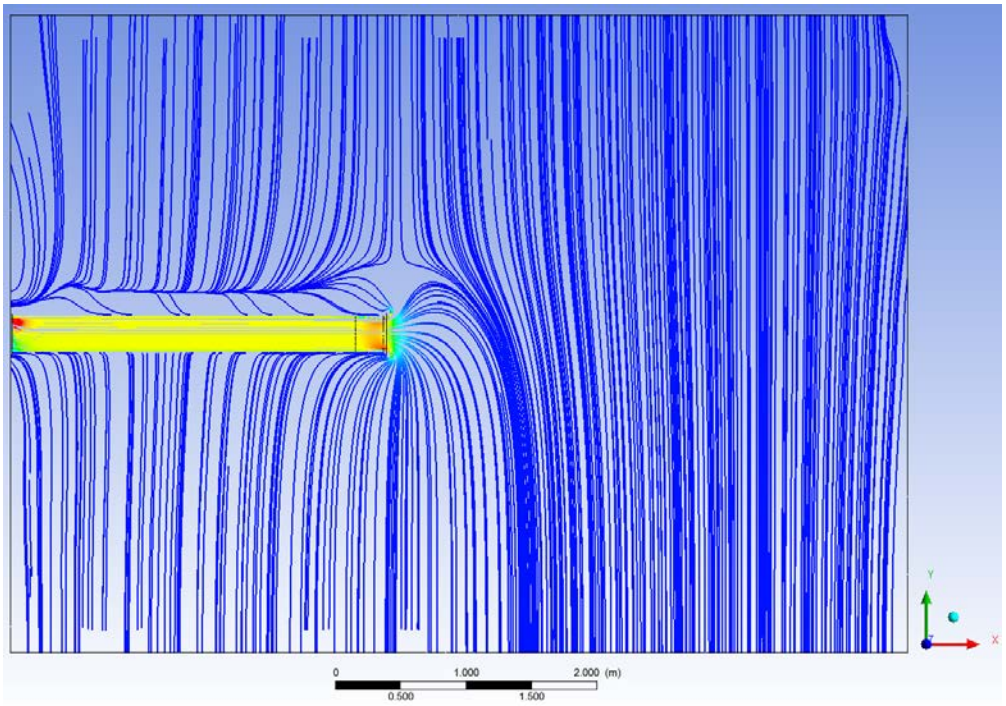

Figure 32: Free field, Full Mass Flow, 90° Crosswind

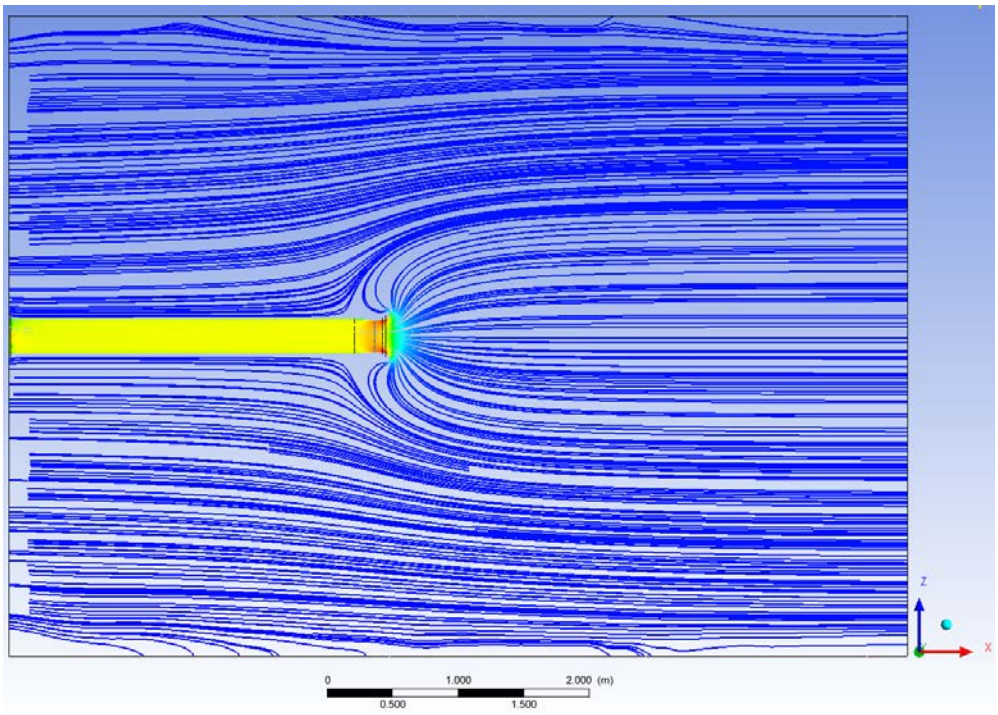

Figure 33: Free field, Full Mass Flow, Headwind

The streamlines behave in the manner expected for the respective crosswind conditions. The velocity contour plots can be found in Appendix B. The average bellmouth velocity values for both configurations were approximately 141 m/s. This value has a difference of 6.6% lower than the average experimental results. In order to improve the results more iterations are needed.

These configurations were repeated with the mass flow set at cruise conditions. The streamline and velocity contour plots can be found in Appendix B. The velocity streamlines were consistent to those in the full mass flow conditions. The average bellmouth velocities were found to be 100 m/s, which correspond to the experimental results.

6.2 20” Centerline Results

As mentioned in Section 5.1, to create the 9.5 inch and 20 inch centerline height domains, the floor was lowered from the original free field model. An error was made during the transfer during this process for the 20 inch centerline height, leading to the computational model not converging to a solution. Shown in Figure 34 are the velocity streamlines for full velocity, no crosswind conditions. The streamlines can be seen to come from the aft and forward walls and be pulled into the ceiling instead of the engine. The model was analyzed in ANSA and multiple meshes were generated, however, the simulation provided the same incorrect results. It was determined the whole domain would have to be remeshed in order to resolve the error. Due to time constraints this was unable to be completed and include in future work.

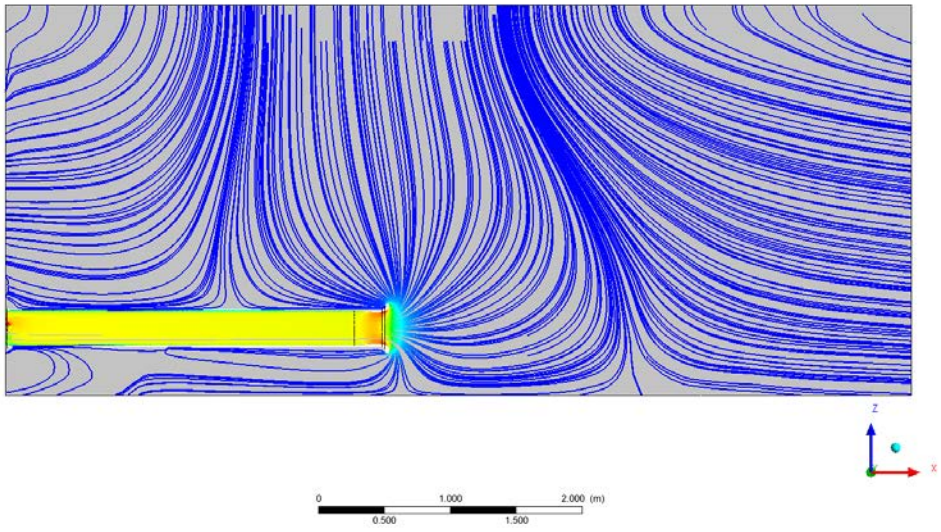

Figure 34: 20", No Crosswind, Full Mass Flow, with Broken Meshing

6.3 9.5” Centerline Results

The 9.5” centerline was successfully run for a full thrust, 90˚ crosswind configuration. The velocity streamlines for this configuration are displayed in Figure 35. On the left-hand side of the figure, streamlines can be seen entering the domain from the forward wall and immediately exiting through the ceiling. This is similar to the results seen in Figure 34, however, this occurred approximately nine feet from the bellmouth inlet. As discussed earlier, only eight feet were required to allow the flow field to fully develop experimentally. Since the flow field behaves as expected 8 feet away in the simulation this result was deemed correct in the immediate region of interest around the bellmouth

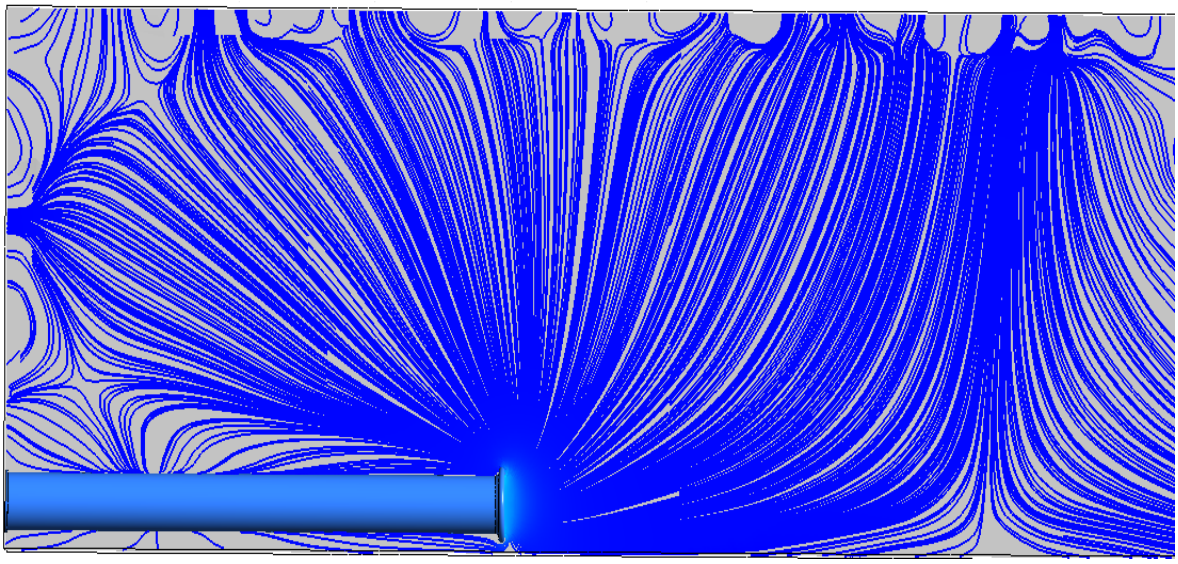

Figure 35: 9.5" CL, Full Mass Flow, Velocity Streamlines

The velocity contours for the engine inlet are shown in Figure 36. The velocity at the bellmouth inlet was shown to be approximately 145 m/s, within the range of experimental results.

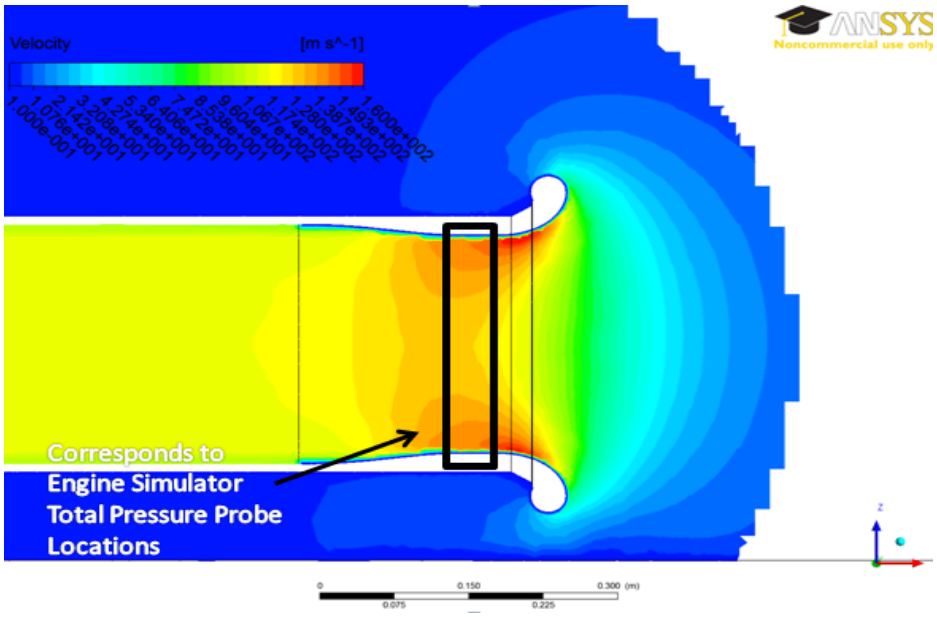

Figure 36: 9.5" CL, Full Mass Flow, Velocity Contour

The results were analyzed to determine vortex formation. Displaying the vortex through the use of three dimensional streamlines was unable to adequately show the characteristics of a vortex. A technique implemented to display the vortex was to plot vorticity, also known as velocity curl and is twice the angular velocity of the flow, displays fluid rotation. The vorticity was plotted for both the non-vortex and vortex forming conditions in Figure 37 and Figure 38, respectively. The vorticity is relatively constant throughout Figure 37 except in the boundary layer. However, in Figure 38 there is a vortex shaped stream of vorticity going from the ground upward and into the engine inlet, demonstrating that a vortex did form.

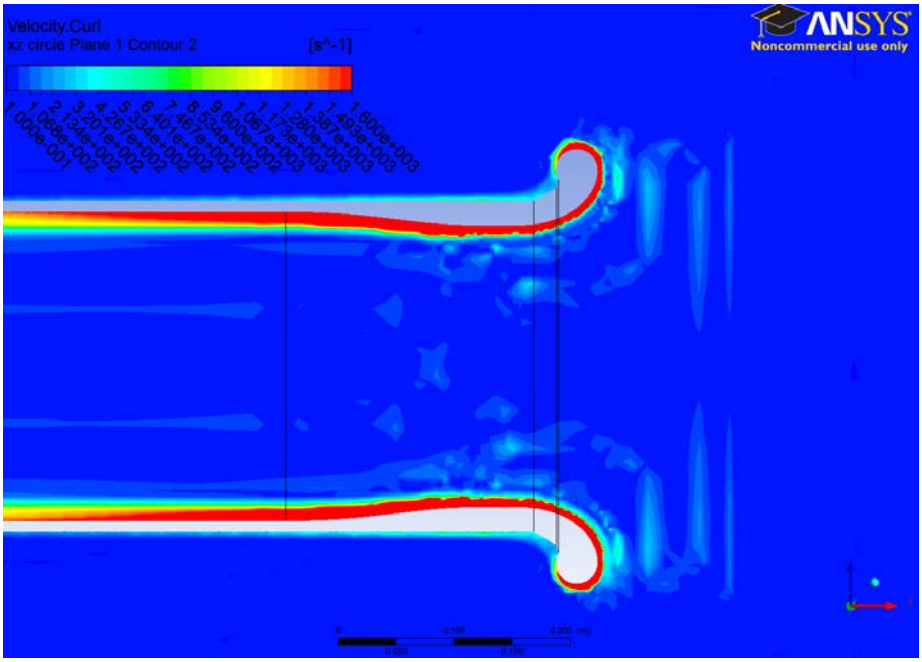

Figure 37: Free Field, Full Mass Flow, No Crosswinds, Velocity Curl Contour

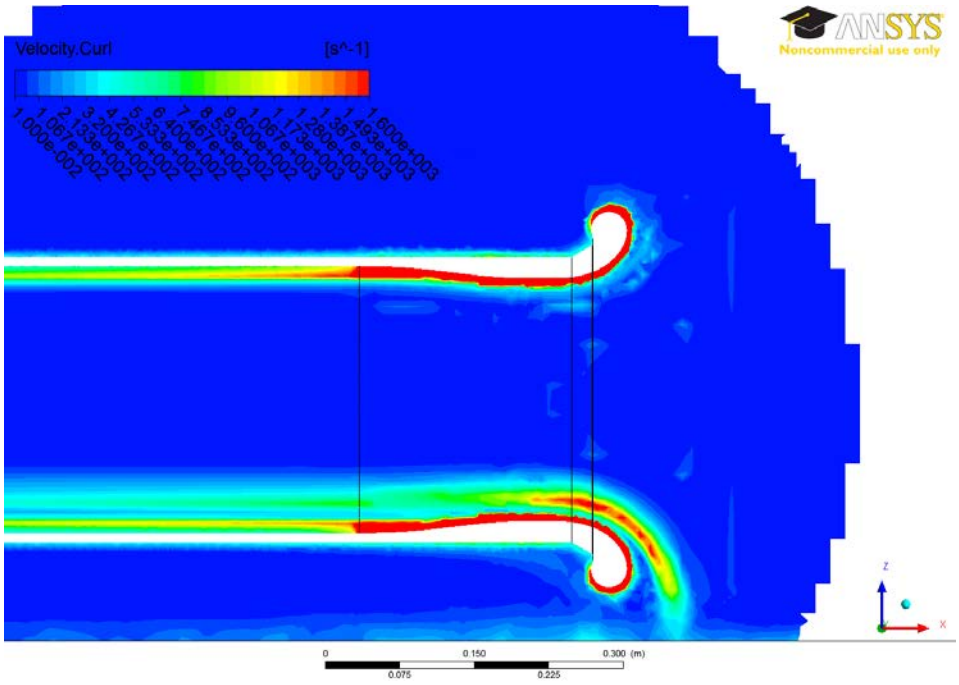

Figure 38: 9.5" CL Full Mass Flow, Crosswinds, Velocity Curl Contour

Another method of showing the formation of a vortex is to plot the surface velocity streamlines on a plane between the engine inlet and the ground plane. If a vortex formed during a simulation then swirl would be seen with the velocity increasing toward the center. This can be seen in Figure 39 for this configuration.

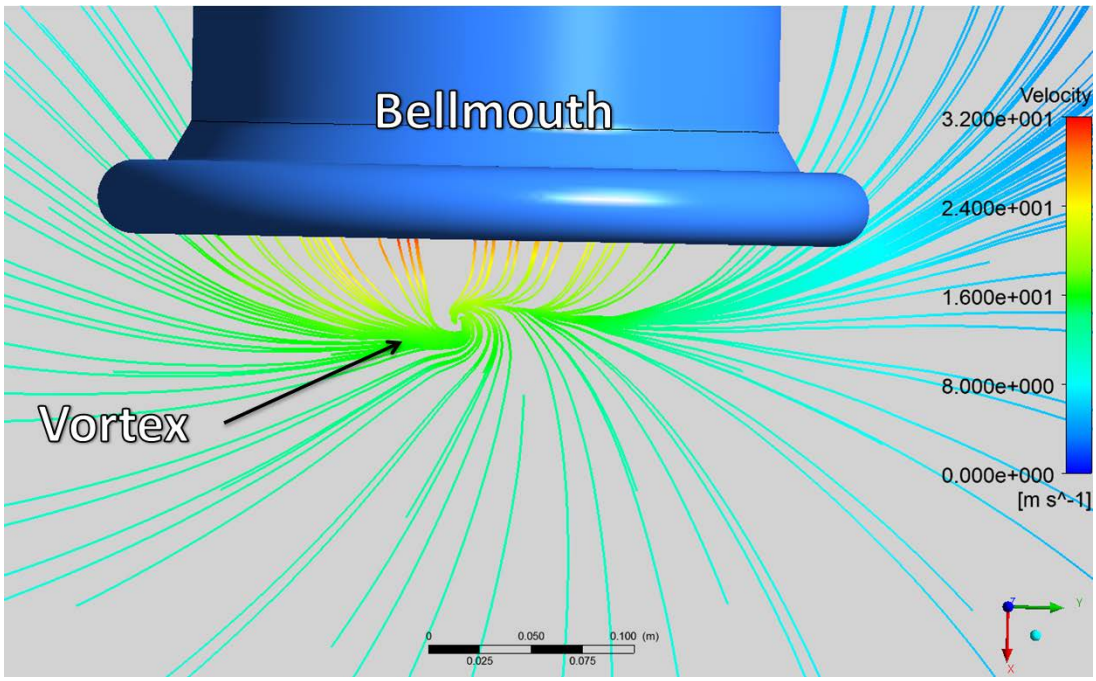

Figure 39: 9.5" CL, Full Mass Flow, 90˚ Crosswind

The full mass flow, headwind configuration was simulated and the inlet velocities matched experimental results. No vortex formation took place. It is possible that the simulation would have formed a vortex after running for a longer period of time due to the complex flow environment and possible that the engine bellmouth geometry may

have delayed the formation of a vortex. To confirm this hypothesis more research would need to be performed.

Chapter 7: Conclusions and Future Work

7.1 Conclusions

The SST k-ω modeler was able to successfully simulate both free field conditions and 9.5 inch centerline height conditions. A vortex was also simulated in CFD using this model. However, the modeler chosen was unable to properly model the pressure distributions at the bellmouth. The flow field also had unexplained anomalies that need to be investigated.

A turbulence modeler should be used that will correctly calculate the pressure distortion with a resolution comparable to experimental results. This will allow direct bellmouth distortion comparisons. A more complex modeler will require greater computational time, however, the CFD results should have a finer solution resolution.

7.2 Summary

Vortex formation can have potentially damaging effects on jet engines. The goal of this research was to computationally analyze the inlet flow of an engine simulator under conditions in which a vortex could form. The computational results were then to be compared to experimental results for corresponding engine configurations as validation.

The results from this research will assist in providing a strong foundation for future computational modeling of vortex formation.

Multiple vortices were captured experimentally at varying 9.5 inch centerline height configurations. A vortex was also computationally formed for the 9.5 inch centerline height with a 90˚ crosswind at full mass flow conditions. The bellmouth velocities were verified with the corresponding experimental settings and the vortex behavior was as expected.

7.3 Future Work

Both the hysteresis and geometry effect on the correlation line are areas with limited research. The CFD completed in this research could be expanded to study these phenomena on vortex formation. Various $\frac{V_i}{V_o}$ and $\frac{H}{D}$ configurations can be simulated in CFD and a new computationally calculated correlation line formed. This would provide a stronger basis for vortex formation conditions and a guideline for future research projects.

References

1. Ho, W., *A Consolidated Study Regarding the Formation of the Aero-Inlet Vortex.* Advances in Intelligent Modelling and Simulation, 2012: p. 345-364.
2. Jermy, M. and W. Ho, *Location of the vortex formation threshold at suction inlets near ground planes by computational fluid dynamics simulation.* Proceedings of the Institution of Mechanical Engineers, Part G: Journal of Aerospace Engineering, 2008. **222**(3): p. 393-402.
3. Gustavo Trapp, L. and R. da Motta Girardi, *Crosswind Effects on Engine Inlets: The Inlet Vortex.* Journal of aircraft, 2010. **47**(2): p. 577-590.
4. Campbell, J.F., et. *al, Patterns in the Sky: Natural Visualization of Aircraft Flow Fields.* NASA Langley Research Center, 1994.
5. Celli, V. *Circulation, vorticity, and vortices*. 1997 Sep 10 1997 [cited 2013 3/10/13]; Available from: http://galileo.phys.virginia.edu/classes/311/notes/fluids1/fluids11/node8.html.
6. Ho, W.H., *Location of Vortex Formation Threshold at Suctin Inlets near Ground Planes- Ascending and Descending Conditions.* World Academy of Science, Engineering and Technology, 2011.
7. Klein, H.J., *Vortex inhibitor for aircraft jet engines*, 1959, Google Patents.
8. Philip Hill, C.P., *Mechanics and Thermodynamics of Propulsion*. Second ed1992: Addison-Wesley Publishing Company, Inc.
9. Rodert, L.A. and F.B. Garrett, *Ingestion of foreign objects into turbine engines by vortices*, in *NACA TN-3330*1955: Washington, D.C.
10. Freuler, R.J., *An investigation of Jet Engine Test Cell Aerodynamics By Means of Scale Model Test Studies with Comparisons to Full-Scale Test Results*, in *Aeronautical and Astronautical Engineering*, The Ohio State University 1991.
11. Montgomery, K.A., *The Design, Instrumentation, and Operation of a Free Field Test Stand For A Scale Model Turbofan Simulator*, in *Aeronautical and Astronautical Engineering*, The Ohio State University 1990. p. 219.
12. Boeing. *Airplane Description*. 2009; Available from: http://www.boeing.com/assets/pdf/commercial/airports/acaps/777rsec2.pdf.
13. Engineering, Validyne. *DP15 Pressure Measurement Systems on Validyne Engineering Sales Corp.*
14. Engineering, Validyne. *CD15 Sine Wave Carrier Demodulators on Validyne Engineering Sales Corp.*
15. ARP, S., *Gas turbine engine inlet flow distortion guidelines.* 2002.
16. Pressure Systems, INC. *Ethernet Intelligent Pressure Scanner*. 2009.
17. *ANSI and IEC Color Codes for Thermocouples, Wire and Connectors*. 2004.
18. Jr., J.D.A., *Computational Fluid Dynamics The Basics With Applications*, New Delhi: McGraw-Hill 2012.
19. Fluent, *Fluent V14.0 Help Files.* 2013.

Appendix A: Additional Experimental Results

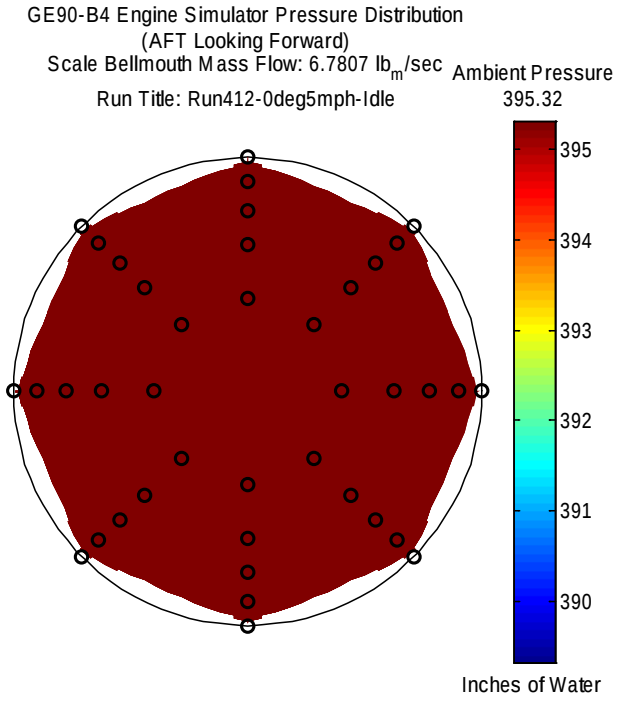

Figure 40: 9.5", Total Pressure Distribution, No Vortex

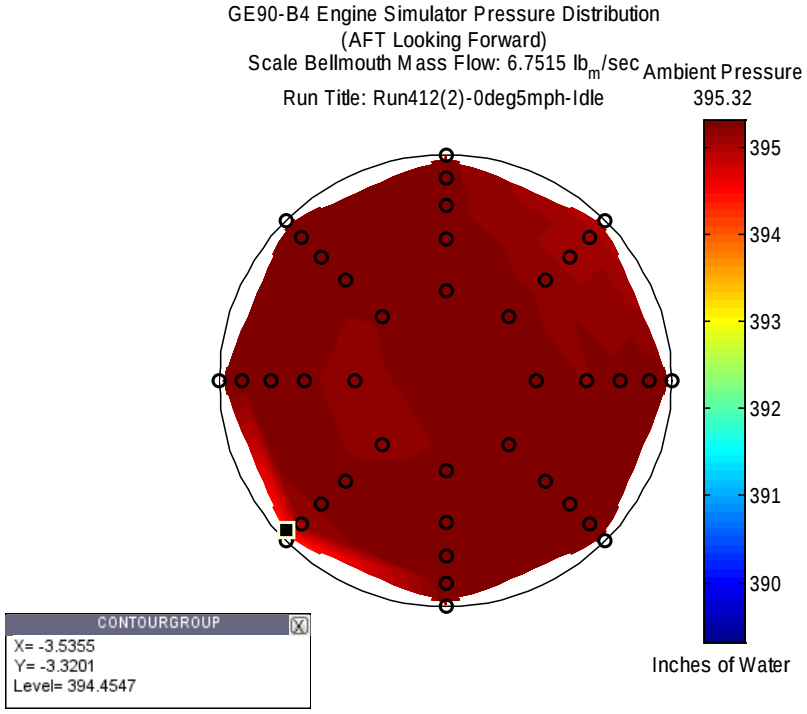

Figure 41: 9.5", Total Pressure Distribution, Vortex Capture

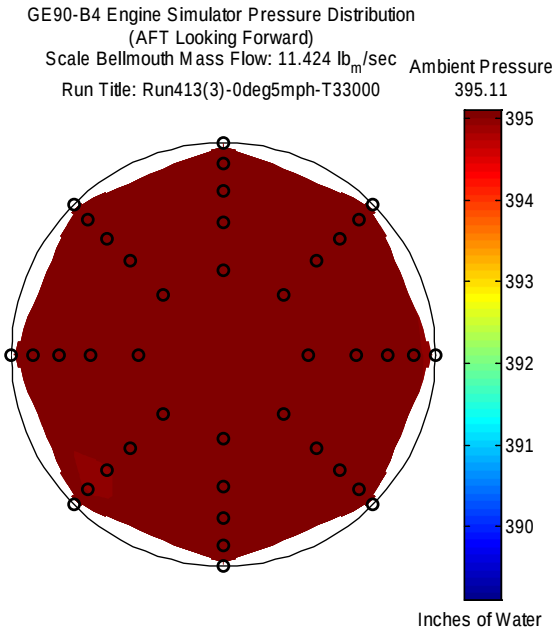

Figure 42: 9.5", Total Pressure Distribution, No Vortex

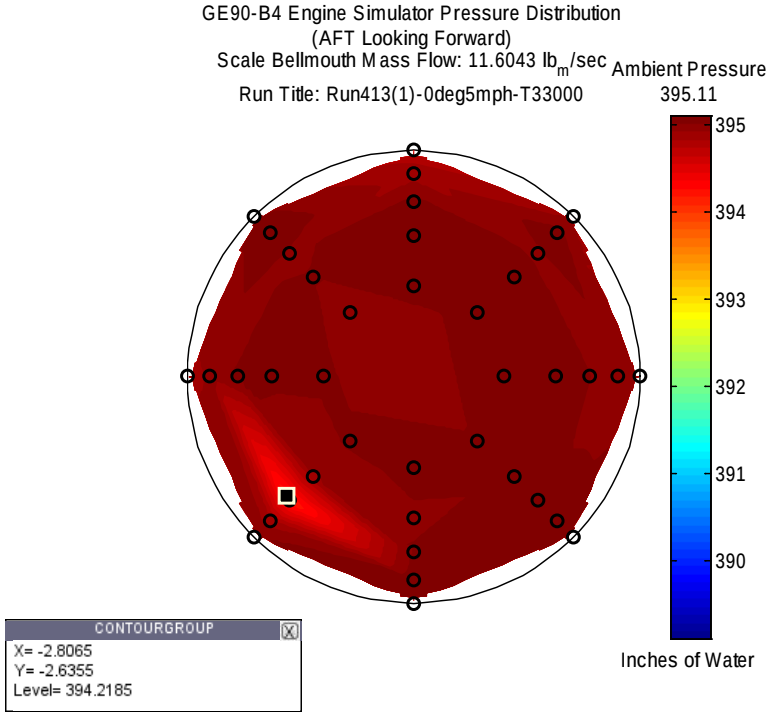

Figure 43: 9.5", Total Pressure Distribution, Vortex Capture

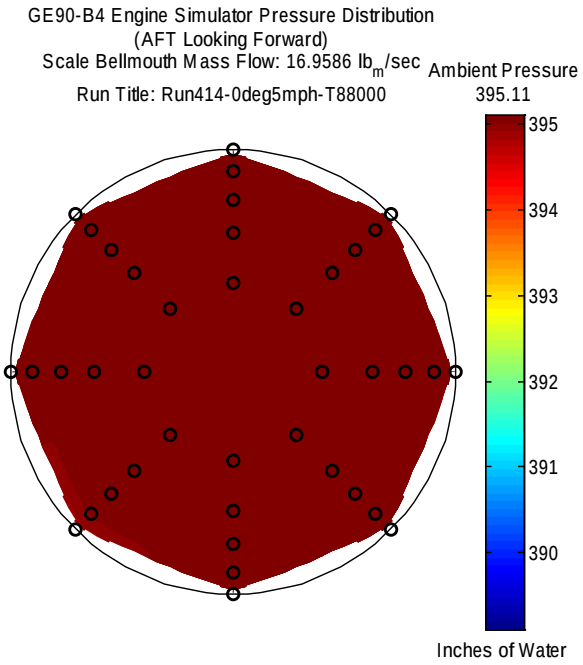

Figure 44: 9.5", Total Pressure Distribution, No Vortex

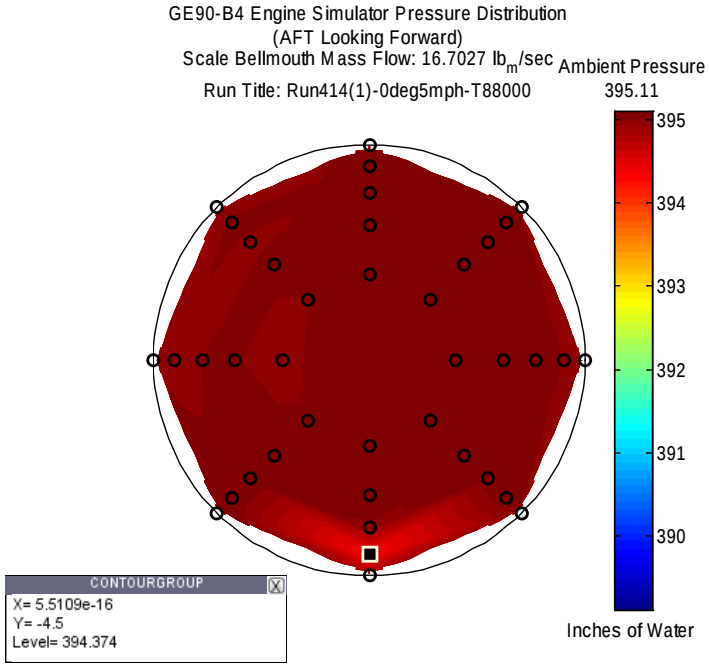

Figure 45: 9.5", Total Pressure Distribution, Vortex Capture

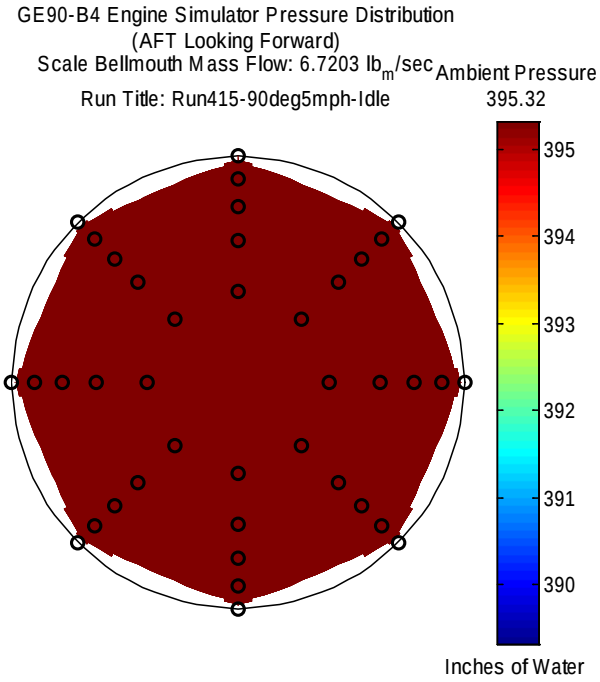

Figure 46: 9.5", Total Pressure Distribution, No Vortex

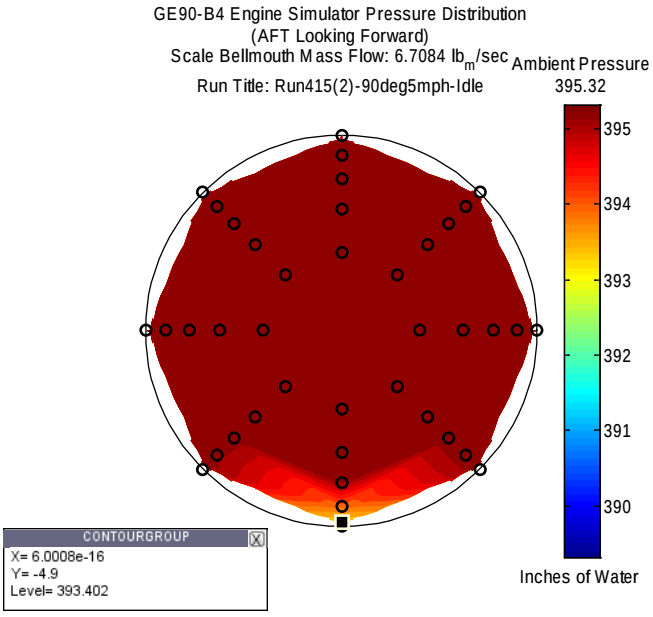

Figure 47: 9.5", Total Pressure Distribution, Vortex Capture

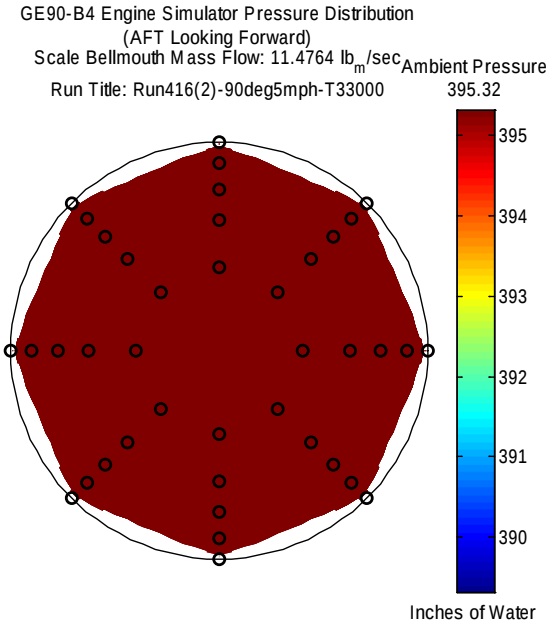

Figure 48: 9.5", Total Pressure Distribution, No Vortex

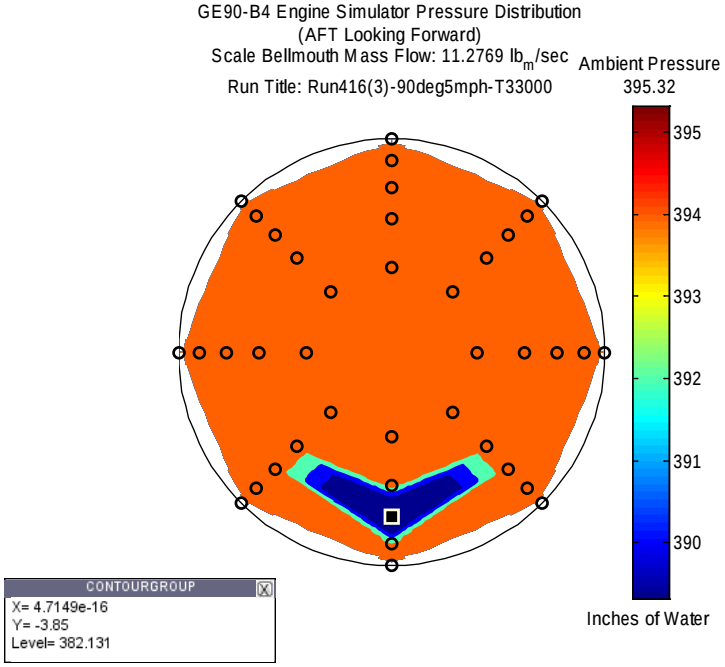

Figure 49: 9.5", Total Pressure Distribution, Vortex Capture

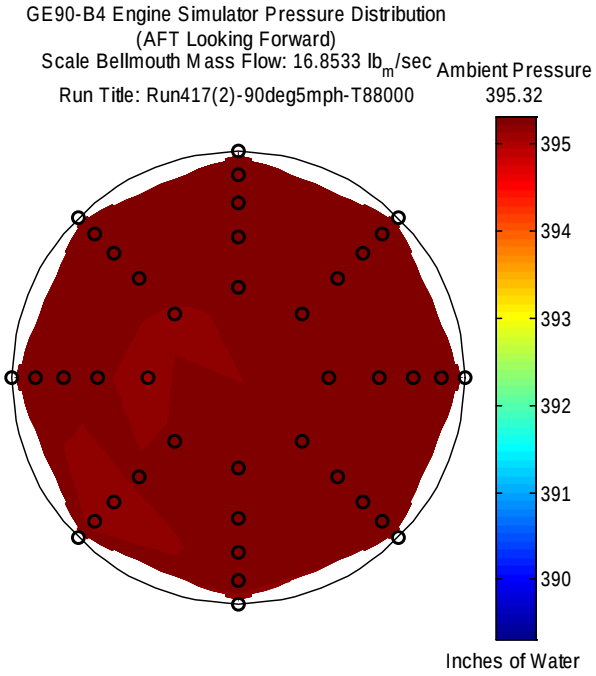

Figure 50: 9.5”, Total Pressure Distribution, No Vortex

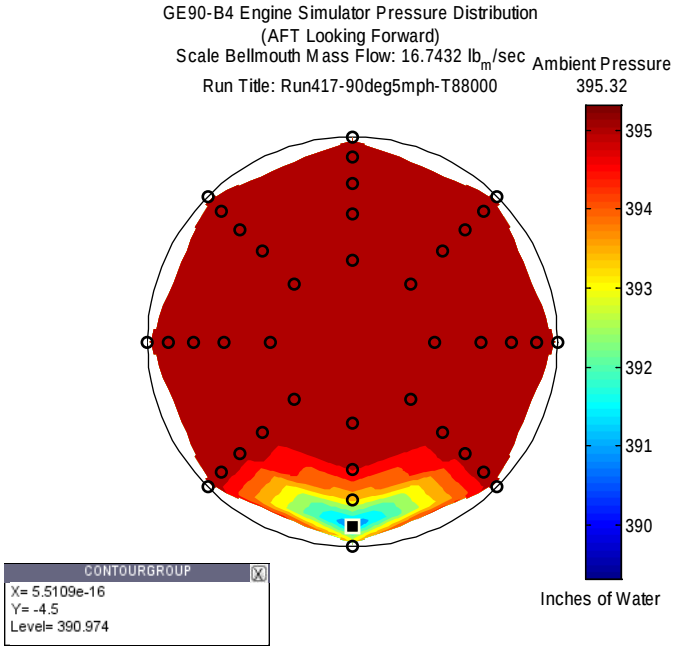

Figure 51: 9.5”, Total Pressure Distribution, Vortex Capture

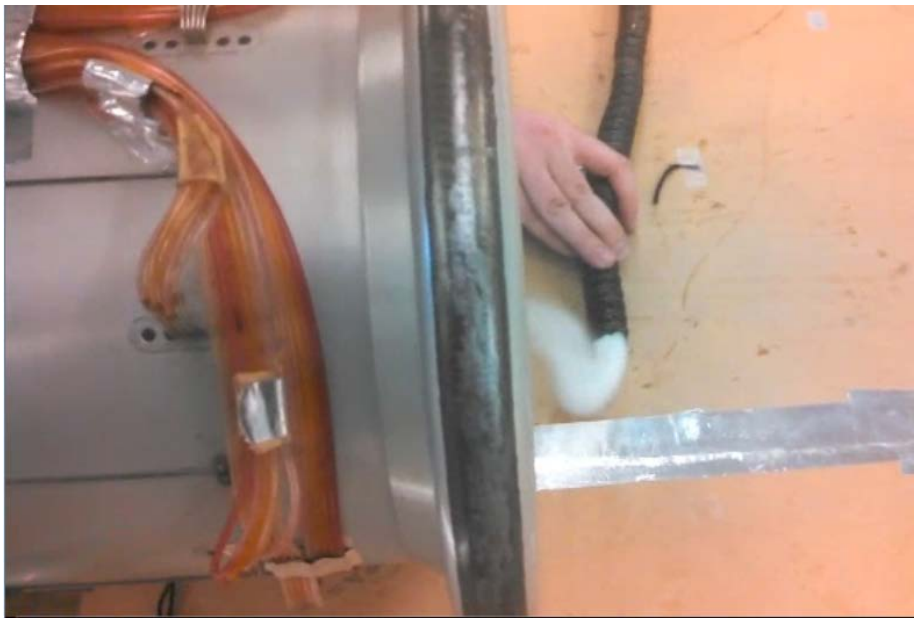

Figure 52: 9.5" CL, Cruise Velocity, Smoke Vortex

Figure 53: 9.5" CL, Idle Velocity, Smoke Vortex

Figure 54: 9.5" CL, Idle Velocity, Tuft Vortex

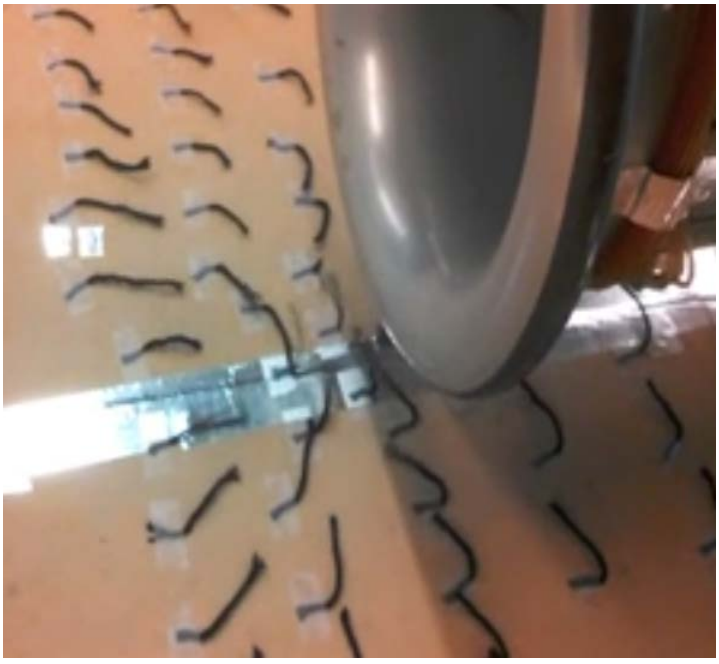

Figure 55: 9.5" CL, Idle Velocity, Moving Tuft Vortex

Appendix B: Additional Computational Results

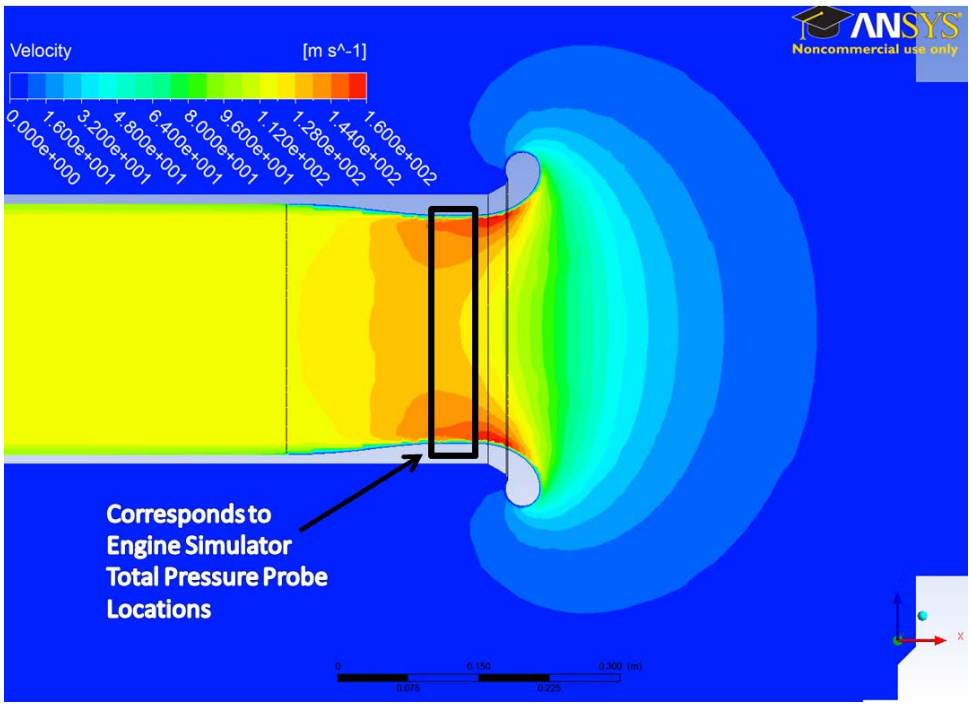

Figure 56: Free Field, Full Mass Flow, 90° Crosswind Velocity Contour

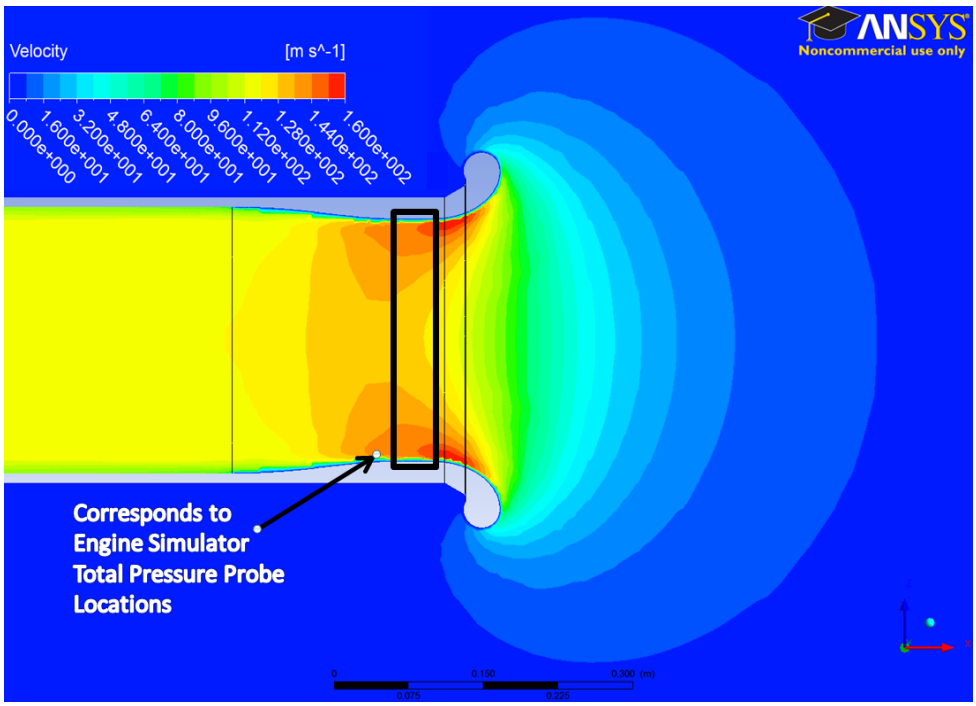

Figure 57: Free Field, Full Mass Flow, Headwind Velocity Contour

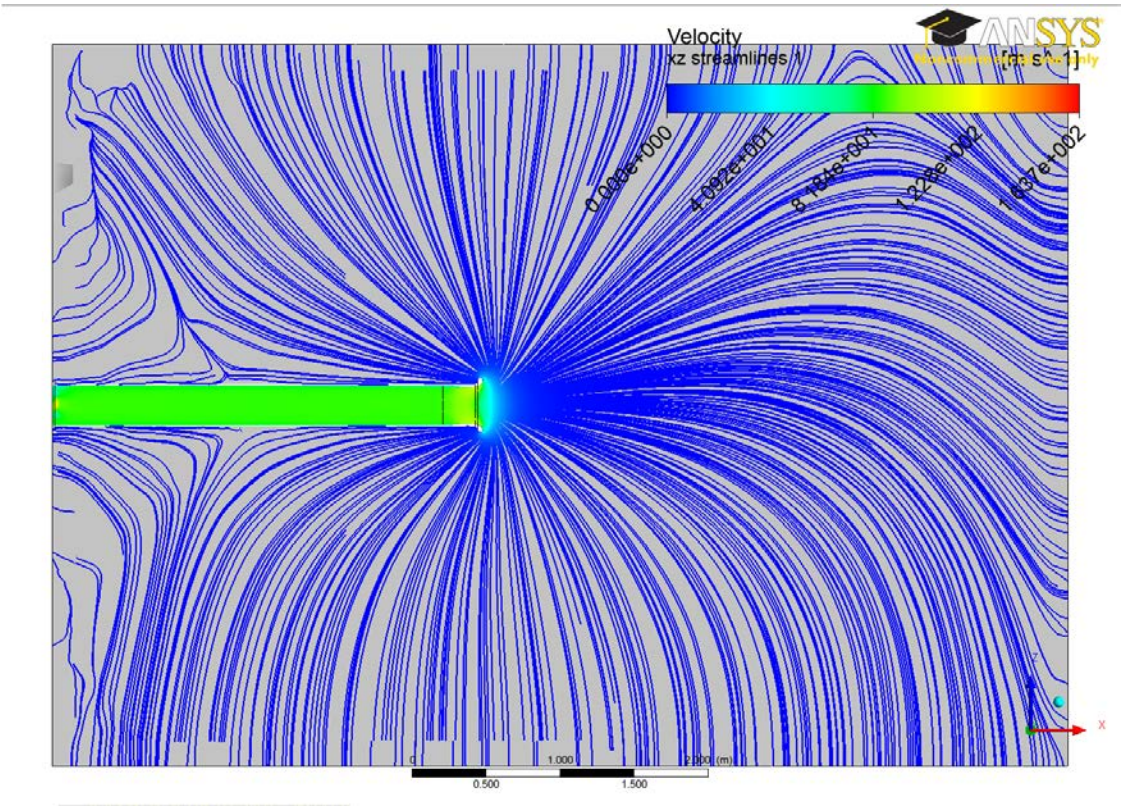

Figure 58: Free Field, Cruise Mass Flow, No Crosswind Velocity Streamlines

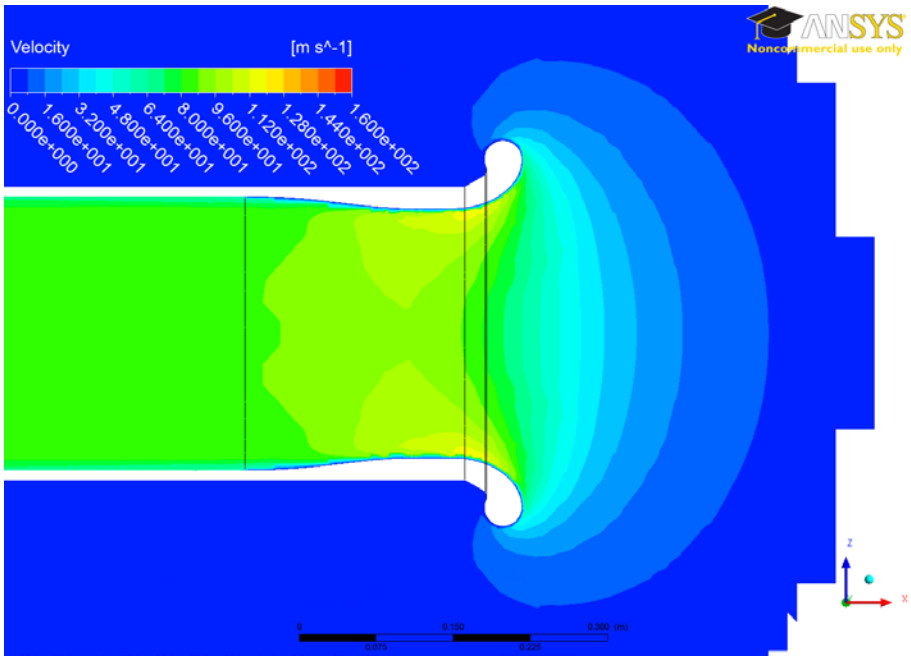

Figure 59: Free Field, Cruise Mass Flow, No Crosswind Velocity Contour

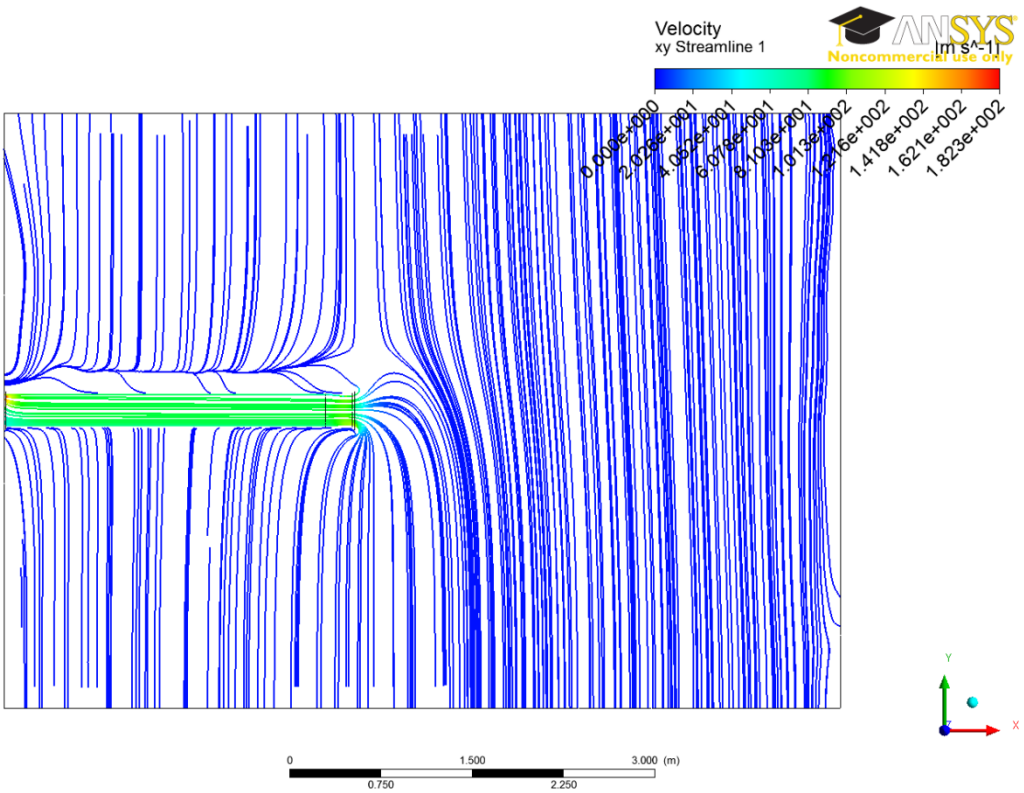

Figure 60: Free Field, Cruise Mass Flow, 90° Crosswind Velocity Streamlines

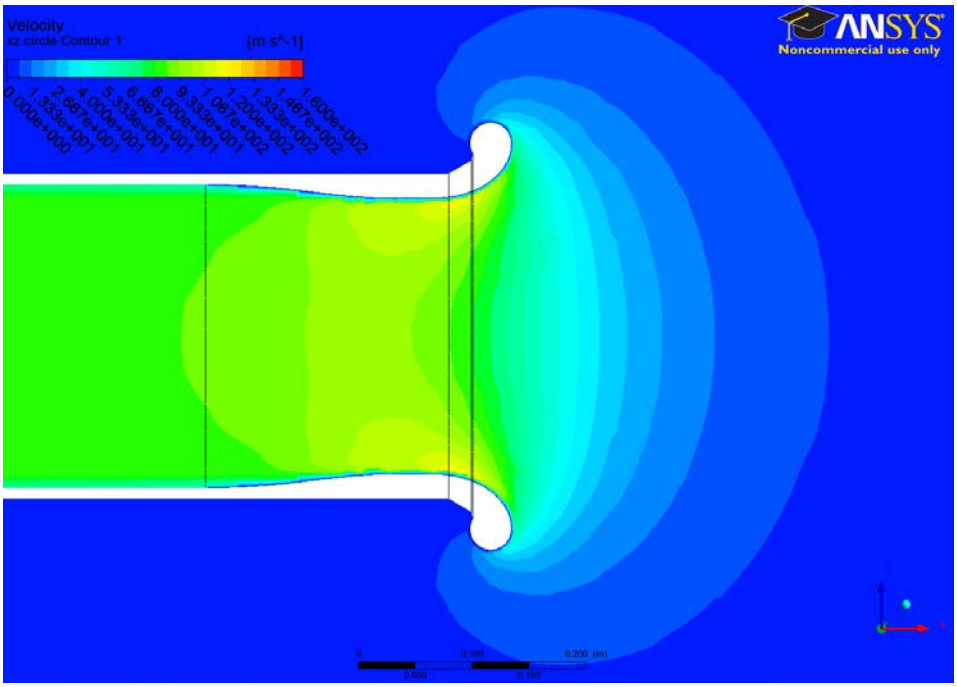

Figure 61: Free Field, Cruise Mass Flow, 90° Crosswind Velocity Contour

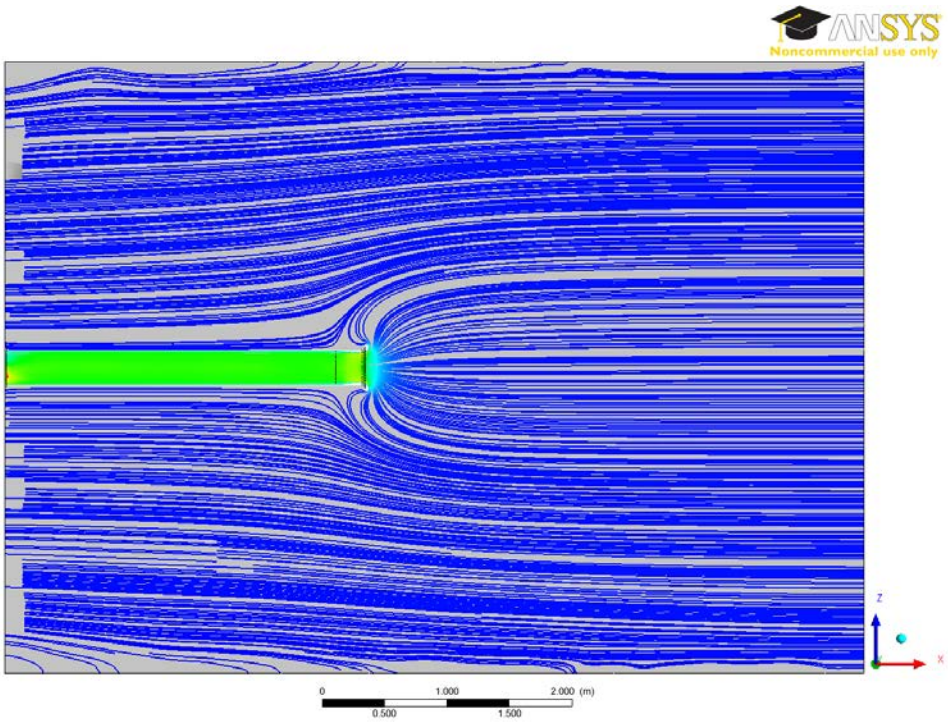

Figure 62: Free Field, Cruise Mass Flow, Headwind Velocity Streamlines

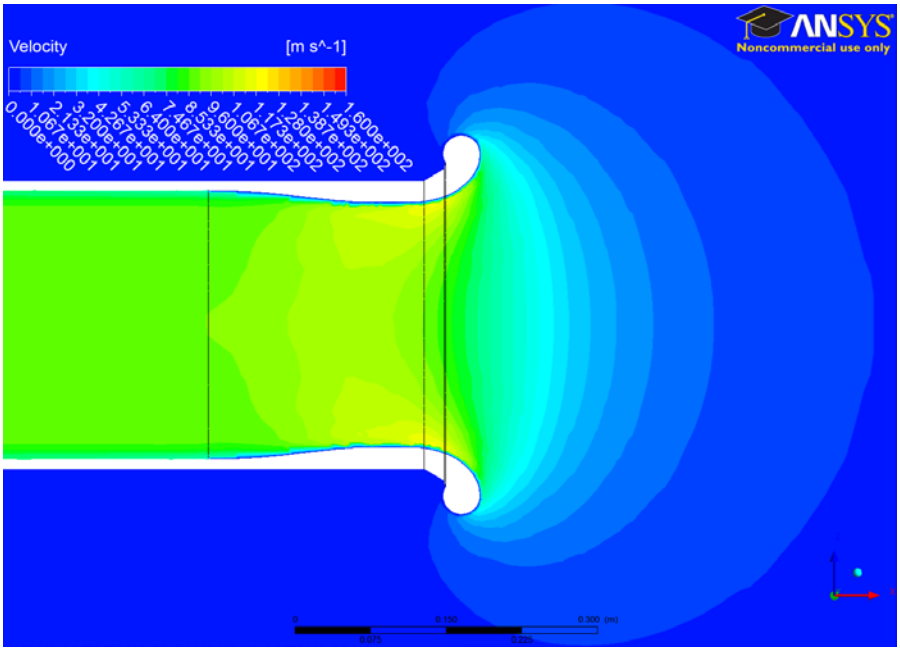

Figure 63: Free Field, Cruise Mass Flow, Headwind Velocity Contour